DRR

[redacted]

UNIVERSITY of PENNSYLVANIA

The Towne School

of

Civil and Mechanical Engineering

PHILADELPHIA, PENNSYLVANIA 19104

RESEARCH FOR THE IMPROVEMENT OF SILICON SOLAR CELL EFFICIENCY

INSTITUTE FOR DIRECT ENERGY CONVERSION

TOWNE SCHOOL

UNIVERSITY OF PENNSYLVANIA
PHILADELPHIA, PENNSYLVANIA

RESEARCH FOR THE IMPROVEMENT OF SILICON SOLAR CELL EFFICIENCY

STATUS REPORT
SR 18

Period Covered: January 1, 1971 to June 30, 1971

Author: M. Wolf

NATIONAL AERONAUTICS AND SPACE ADMINISTRATION
GRANT NGL-39-010-001

JULY 1971

TABLE OF CONTENTS

I INTRODUCTION

This report describes the work performed during the second semi-annual period under contract NGL-39-010-001. The work performed is partially a continuation and completion of work started in the first reporting period. Besides, new work has been started primarily in the direction of gaining additional understanding of the theoretical relationships determining the current-voltage characteristic of silicon solar cells.

The calculations performed in the first reporting period to generate design data for the light generated current in dependence on material and physical device parameters have lead to the statement in the report covering the first period, that the data might lend themselves to the preparation of a "solar cell design handbook". Although the design data obtained during that period fulfilled the requirements of the present contract, it was felt desireable to rework these data and augment them by additional data to form the beginning of such a design handbook. Also, it was thought desireable to appropriately explain the mathematical basis on which such design curves are based. This has been done, and section 2 of this report contains essentially the first section of this "design handbook", dealing with the collection efficiency part of the design tasks.

Since certain recommendations arose from the design calculations carried out relative to the collection efficiency, it was found also desireable to first investigate the effect of such structure changes on the current-voltage characteristic. This investigation has been carried out, and the existing theoretical relationships for diffusion current contributions from the base region and the diffused region have been expanded to cover the two-layer model including drift fields, analogous to that used for the calculations of collection efficiency.

A new computer program has been generated based on the new theoretical relationships, and design calculations have been carried out. Although the evaluations of these calculations is not complete, preliminary investigation of the data indicates that any structural and material parameter measures taken to improve the collection efficiency also reduce the dark diode current, and thus improve the current-voltage characteristic.

A computer program for the reduction of experimental data on the current-voltage characteristic of solar cells has been described in the first semi-annual report. Further work on this program has been carried out, and has led to successful completion. The program has been found extremely useful, saving not only considerable amounts of time in the reduction of such data, but also providing an accuracy in determining the 5 constants of the two-exponential current-voltage characteristic, not possible by any other method. Use of this program on a relatively small number of cells so far has led to the conclusion that the two-exponential relationship appears to be the appropriate one to describe the current-voltage characteristic of silicon solar cells. Comments on the practice of reduction of computer data on the experimental current-voltage characteristic, a description of the computer program and of its use, and some results obtained with it are discussed in section 4 of this report.

The experimental effort towards verification of the collection efficiency improvement in the short wavelength region by reduction of the surface recombination velocity and reduction of the diffused region thickness has been delayed, since a similar program has been carried out at Comsat Laboratories. The program there has been extremely successful, and has led to verification of the predictions made in the beginnings of this program.

II THE "SILICON SOLAR CELL DESIGN HANDBOOK"

1 Introduction

This is the first part of an endeavor to create a "silicon solar cell design handbook". Through such a handbook, it should become possible to reduce solar cell design from an art and science to an engineering task. This objective can be accomplished by either of two methods: in the old-fashioned way of presenting design curves and data tables, and the modern way of computerized design. Here, a time-inverted approach is used, primarily for instructional purposes: the computer has been used to provide the data from which design curves have been prepared. From the design curves, it is easier to gleen the influence of the various design parameters, than it would be from the results of a computer design program which yields the optimized design data directly. Getting a feel for the influence of the various material and dimensional parameters of the device, and of their interrelationships is still important at the present stage of development.

A design process in general consists of an analysis and a synthesis. In the analysis part, the influence of material and design parameters on each component, subsystem, or performance attribute is established. In the synthesis part, these elements are combined to provide the overall performance of the system, possibly necessitating recycling through the first stage to provide an optimized design.

The design approach is logically split into three parts, concerned with the light generated current, the open circuit voltage, and the fill factor. A principal measure of performance relative to the light generated current is the collection efficiency. The collection efficiency is strongly influenced by the spectral distribution of the incoming light. The following design data for collection efficiency are restricted to airmass zero sunlight. Since open circuit voltage and fill factor are not dependent on the spectral distribution, at least in the commonly used silicon solar cells, the design data relating to these two quantities are of broader validity.

2. The Basis for the Collection Efficiency Design Curves

In order to perform such an analysis and synthesis, it appears most practical to break the total task into logical parts. This can be done by starting from the governing performance criterion, the efficiency for solar energy conversion, following well established practices for the most part. Overall conversion efficiency of a solar cell, like any efficiency, is determined by the relationship:

$$\eta = \frac{P_{out}}{P_{in}} \quad ; \tag{1}$$

where:

$$P_{in} = \int_0^\infty P_{in}(\lambda)\, d\lambda \; ; \tag{2}$$

integrated over all wavelengths comprising the intensity spectrum of the light incident upon the cell. (ref.1) The maximum output power available is the product of a current density and a voltage:

$$P_{out} = j_{max} \cdot V_{max} \tag{3}$$

Here, all power values and the current density have been referred to unit area of light-exposed cell-surface. The power output has been related to the light generated current and the energy gap by means of two factors:

$$P_{out} = j_L \cdot E_G \cdot (V.F.) \cdot (F.F.) \; ; \tag{4}$$

where: $(V.F.) = \frac{V_{oc}}{E_G}$; (4a)

and: $(F.F.) = \frac{j_{max} \cdot V_{max}}{j_L \cdot V_{oc}}$ (4b)

(V.F.), called the "voltage factor", and (F.F.), called the "fill factor", are largely determined by the characteristic of the rectifying potential barrier of the device (in the Si solar cell: a pn-junction). However, shunt current and series resistance effects can degrade both factors below those which are based on the characteristics of the barrier itself. As a result of this observation, the voltage factor is best described as a product: $(V.F.) = (V.F.)_J \cdot (V.F.)_A$.

The subscript "J" refers to the voltage factor as it would be obtained in an "ideal" solar cell, where only the characteristic of the rectifying potential barrier of the device determines the open circuit voltage. However, artefacts such as process or design effects which result in effective shunt currents, can lower the open circuit voltage. These effects are lumped in the second voltage factor designated by subscript "A". In silicon solar cells, the shunt currents have generally been reduced to the point where they have negligible influence on the open circuit voltage. Therefore, $(V.F.)_A \approx 1$, and only the first factor needs consideration. In this case, the subscript "J" is generally omitted, and the voltage factor understood to be based on the junction characteristic only.

The Fill-Factor (F.F.) can similarly be broken into 2 factors:

$$(F.F.) = (C.F.) \cdot (A.F.) \tag{4c}$$

where the "Curve Factor" (C.F) has been used in the literature (ref.1) to designate the part based on the characteristics of the potential barrier, and where (A.F.) is introduced herewith to account for additional "softening" of the IV - characteristic, as it is caused by artefacts such as shunting or series resistance.

Thus:
$$\eta = \frac{j_L \quad E_G \; F(J) \quad G(A)}{P_{in}} \; ; \tag{5}$$

where: $F(J) = (V.F.)_J \cdot (C.F.)$ is a function dominated by the potential barrier, being less strongly dependent on j_L, and $G(A) = (V.F.)_A \cdot (A.F.)$ is a function primarily of the artefacts, while j_L depends primarily on the material properties of the diffused and the base regions of the device, and rather little on the parameters of the transition region associated with the potential barrier.

It is:
$$j_L = q \int_0^\infty N_{ph}(\lambda) \gamma(\lambda) \, d\lambda \; ; \tag{6}$$

where $\gamma(\lambda)$ is called the overall collection efficiency, since it relates the number of charge carriers collected and made utilizable in current flow through an outside circuit to the number of photons available for conversion.

It is:

$$P_{in}(\lambda)\, d\lambda = N_{ph}(\lambda)\, E_{ph}(\lambda)\, d\lambda \quad ; \tag{7}$$

or:

$$\doteq N_{ph}(\lambda)\, \frac{hc}{\lambda}\, d\lambda \quad ; \tag{7a}$$

where $N_{ph}(\lambda)$ is the number of photons incident in the wavelength range $d\lambda$ around wavelength λ, h being Planck's constant and c the velocity of light. $E_{ph}(\lambda)$ is the energy of the individual photon of wavelength λ.

Thus:

$$J_L = \frac{q}{hc} \int_0^\infty P_{in}(\lambda)\, g\nu(\lambda)\, \frac{1}{\lambda}\, d\lambda \quad ; \tag{8}$$

Not all of the incident energy is absorbed in the cell: some is reflected from the surface, another part is not absorbed, but effectively transmitted through the device. The reflected energy is:

$$P_{refl}(\lambda) = P_{in}(\lambda) \cdot r(\lambda) \quad ; \tag{9}$$

where $r(\lambda)$ is the reflection coefficient at wavelength λ. The transmitted energy is given by Lambert's law of absorption:

$$P_{tr}(\lambda) = P_o(\lambda)\, e^{-\alpha(\lambda)\, d}; \tag{10}$$

where d is the thickness of the absorbing layer, P_o the energy entering the layer, and $\alpha(\lambda)$ the absorption coefficient at wavelength λ. For simplicity, it is assumed that reflection at the backsurface does not take place.

Then:

$$P_{in}(\lambda) \left[1 - r(\lambda)\right] \left[1 - e^{-\alpha(\lambda)\, d}\right] d\lambda \tag{11}$$

is the energy actually absorbed in the layer of thickness d in the wavelength interval $d\lambda$ at λ. Both relations - for reflection and for absorption --- are generally used for light intensities, or incident energy flux P_{in}. It is seen that they can also be applied to N_{ph}.

Then:

$$J_L = q \int_0^\infty N_{ph}(\lambda) \left[1 - r(\lambda)\right] \left[1 - e^{-\alpha(\lambda) d}\right] \eta_{coll}(\lambda) d\lambda \tag{12}$$

Here, $\eta_{coll}(\lambda)$ is the collection efficiency of the device, related to the number of photons actually absorbed within it. Since useful absorption does not take place beyond the absorption edge, that is absorption with generation of minority carriers, it suffices to extend the integral at its upper limit to a cutoff wavelength λ_G determined by the energy gap of the semiconductor used:

$$\lambda_G = \frac{hc}{E_G} \quad ; \tag{13}$$

The expression for the total light generated current j_L can thus be written in the form:

$$j_L = \int_0^{\lambda_G} j_L(\lambda) d\lambda ; \tag{14}$$

At this point the first assumption will be introduced. It is possible that $\eta_{coll}(\lambda)$ is not only a function of λ, but also of $N_{ph}(\lambda')$, where λ' can be any wavelength other than λ within or outside of the range of integration. If this is the case, the integral is not linear in $N_{ph}(\lambda)$. This will be the case, for instance, if trapping of charge carriers occurs to a significant degree, or if the total incident light intensity P_{in} is so large as to generate a miniority carrier density in any region of the solar cell which is not small compared to the majority carrier density, so that minority carrier lifetime can no longer be considered independent of minority carrier density and, in general, the normal assumptions of small signal theory can not be made. Fortunately, in normal silicon solar cells, and probably in many other types of solar cells, the conditions for validity of the assumption are fulfilled, even for the use of rather large concentration ratios. A device which is known to violate the assumption is the Cu_2S-CdS solar cell. It will therefore be necessary to test the validity of the assumption before applying the relationships to be subsequently developed herein to other types of solar cells. Although the general methods applied here may be useful in these other cases also, modifications of some details will be necessary.

It is practical at this point to introduce weighted average values for the

reflected energy, the energy actually absorbed in the wafer, and the collection efficiency η_{coll}:

$$J_L = -q(1 - R_{refl})\, R_{abs}\, \eta_{coll} \int_0^{\lambda_G} N_{ph}(\lambda)\, d\lambda \; ; \tag{15}$$

where $$\eta_{coll} = \frac{\int_0^{\lambda_G} N_{ph}(\lambda)\, [1 - r(\lambda)]\, [1 - e^{-\alpha(\lambda) d}]\, \eta_{coll}(\lambda)\, d\lambda}{\int_0^{\lambda_G} N_{ph}(\lambda)\, [1 - r(\lambda)]\, [1 - e^{-\alpha(\lambda) d}]\, d\lambda} \; ; \tag{16}$$

The fraction of the energy absorbed in the device to that entering it is given by R_{abs}:

$$R_{abs} = \frac{\int_0^{\lambda_G} N_{ph}(\lambda)\, [1 - r(\lambda)]\, [1 - e^{-\alpha(\lambda) d}]\, d\lambda}{\int_0^{\lambda_G} N_{ph}(\lambda)\, [1 - r(\lambda)]\, d\lambda} \; ; \tag{17}$$

while the reflected energy is:

$$R_{refl} = \frac{\int_0^{\lambda_G} N_{ph}(\lambda)\, [1 - r(\lambda)]\, d\lambda}{\int_0^{\lambda_G} N_{ph}(\lambda)\, d\lambda} \; ; \tag{18}$$

Since the reflection can, in practice, be reduced to very small values, R_{refl} is assumed to be zero in the following. However, actual reflection characteristics can very readily be introduced into the subsequent equations by replacing $N_{ph}(\lambda)$ with $N_{ph}(\lambda)\, [1 - r(\lambda)]$. Note: if $1 - r(\lambda)$ is significant and has a strong dependence on wavelength, the design curves given in the following will not be accurate and should be re-computed for the specific reflection characteristic.

3. Collection from the 3 major regions of the cell

Since contributions to the light generated current j_L can be identified as originating in three different regions of the solar cell, it is practical to write:

$$j_L = \int_0^{\lambda_G} \left[j_{L,D}(\lambda) + j_{L,T}(\lambda) + j_{L,B}(\lambda) \right] d\lambda \; ; \tag{19}$$

where the subscripts D,T, and B refer to the diffused region, transition region, and base region of the cell, respectively. In the following, it is tacitly assumed, without loss of generality, that the diffused region is the one adjacent to the light exposed surface. If an "inverted" structure should be considered, it is merely necessary to enter the parameters of the diffused region into $\eta_{coll,B}$, and those of the nondiffused region into $\eta_{coll,D}$.

Three collection efficiencies can then be introduced, one each connected with one of the major regions.

$$\begin{aligned} j_L = q \int_0^{\lambda_G} N_{ph}(\lambda) \Big\{ & \left[1 - e^{-\alpha(\lambda)\, x_{T,F}} \right] \eta_{coll,D} \\ & + \left[e^{-\alpha(\lambda)\, x_{T,F}} - e^{-\alpha(\lambda)\, x_{T,R}} \right] \eta_{coll,T} \\ & + \left[e^{-\alpha(\lambda)\, x_{T,R}} - e^{-\alpha(\lambda)\, d} \right] \eta_{coll,B} \Big\} d\lambda \; ; \end{aligned} \tag{20}$$

Here, $x_{T,F}$ is the location of the front boundary of the transition region (depletion region), that is the one situated more closely to the light exposed surface of the device, to which x = 0 has been assigned. A second assumption has been made here, containing the condition that the entire structure is plane-parallel so that all surfaces of significance are planes and are parallel to the light exposed surface. Not included in this parallelity condition are obviously

the surfaces which form the edges of the wafer.

$x_{T,R}$ is the location of the rear boundary surface of the transition region.

Equation (20) can be written as three separate integrals, designating the light generated current contributions from the three regions:

$$j_L = j_{L,D} + j_{L,T} + j_{L,B}; \tag{20a}$$

Then:
$$j_L = q \int_0^{\lambda_G} N_{ph}(\lambda) \left[1 - e^{-\alpha(\lambda) x_{T,F}}\right] \eta_{coll,D}(\lambda)\, d\lambda; \tag{21}$$

$$= q R_{abs} R_D \eta_{coll,D} \int_0^{\lambda_G} N_{ph}(\lambda)\, d(\lambda);$$

where:
$$\eta_{coll,D} = \frac{\int_0^{\lambda_G} N_{ph}(\lambda) \left[1 - e^{-\alpha(\lambda) x_{T,F}}\right] \eta_{coll,D}(\lambda)\, d\lambda}{\int_0^{\lambda_G} N_{ph}(\lambda) \left[1 - e^{-\alpha(\lambda) x_{T,F}}\right] d\lambda}; \tag{21a}$$

and:
$$R_D = \frac{\int_0^{\lambda_G} N_{ph}(\lambda) \left[1 - e^{-\alpha(\lambda) x_{T,F}}\right] d\lambda}{\int_0^{\lambda_G} N_{ph}(\lambda) \left[1 - e^{-\alpha(\lambda) d}\right] d\lambda}; \tag{21b}$$

Similarly:
$$j_{L,B} = q R_{abs} R_B \eta_{coll,B} \int_0^{\lambda_G} N_{ph}(\lambda)\, d\lambda; \tag{22}$$

with

$$\eta_{coll,B} = \frac{\int_0^{\lambda_G} N_{ph}(\lambda)\left[e^{-\alpha(\lambda)\,x_{T,R}} - e^{-\alpha(\lambda)\,d}\right]\eta_{coll,B}(\lambda)\,d\lambda}{\int_0^{\lambda_G} N_{ph}(\lambda)\left[e^{-\alpha(\lambda)\,x_{T,R}} - e^{-\alpha(\lambda)\,d}\right]d\lambda}\;; \tag{22a}$$

and

$$R_B = \frac{\int_0^{\lambda_G} N_{ph}(\lambda)\left[e^{-\alpha(\lambda)\,x_{T,R}} - e^{-\alpha(\lambda)\,d}\right]d\lambda}{\int_0^{\lambda_G} N_{ph}(\lambda)\left[1 - e^{-\alpha(\lambda)\,d}\right]d\lambda} \tag{22b}$$

Finally,

$$j_{L,T} = q\;R_{abs}\;R_T\;\eta_{coll,T}\int_0^{\lambda_G} N_{ph}(\lambda)\,d\lambda\;; \tag{23}$$

with

$$\eta_{coll,T} = \frac{\int_0^{\lambda_G} N_{ph}(\lambda)\left[e^{-\alpha(\lambda)\,x_{T,F}} - e^{-\alpha(\lambda)\,x_{T,R}}\right]\eta_{coll,T}(\lambda)\,d\lambda}{\int_0^{\lambda_G} N_{ph}(\lambda)\left[e^{-\alpha(\lambda)\,x_{T,F}} - e^{-\alpha(\lambda)\,x_{T,R}}\right]d\lambda}\;; \tag{23a}$$

and

$$R_T = 1 - R_D - R_B$$

$$= \frac{\int_0^{\lambda_G} N_{ph}(\lambda) \left[e^{-\alpha(\lambda) x_{T,F}} - e^{-\alpha(\lambda) x_{T,R}} \right] d\lambda}{\int_0^{\lambda_G} N_{ph}(\lambda) \left[1 - e^{-\alpha(\lambda) d} \right] d\lambda} \quad ; \tag{23b}$$

With this, now, the foundation has been laid for the presentation of design data for the various aspects or parts of the device. R_{abs} permits evaluation of the direct effect of wafer thickness d on the overall collection efficiency. Introduction of R_D, R_B, and R_T permits separate optimization of the main regions of the solar cell, the design of which can be carried out relatively independently. The performance criteria here are the collection efficiencies for the three regions.

4. The Collection Efficiency Design Curves

Basic to the use of the collection efficiency design curves is the knowledge of R_{abs}, R_D, R_T, and R_B. R_{abs} is given in Fig.II-1 as function of wafer thickness d. R_D and R_B are directly obtained from Fig.II-2, when the transition region thickness of the pn-junction is taken to be zero. If the transition region thickness is not zero, then R_D and R_B are also obtained from Fig.II-2, but in this case, by using $x_{J,F}$ for reading off R_D, instead of x_j as the parameter, and similarly $x_{J,R}$ instead of x_j for obtaining R_B.

R_T is then obtained from

$$R_T = 1 - R_D - R_B \quad ; \tag{24}$$

The collection efficiency of the transition region has been taken as 100% up to this point.

It is important for the user of the Design Handbook to realize the restrictions and assumptions, under which the data have been prepared. It has to be left to him to assure himself, before using the data, that his case at hand does not significantly violate these assumptions. This is the reason why, in the discussion of the previous sub-section, the assumptions made have been stressed, and why, in the following paragraphs, further discussions follow on the assumptions made and on their impact on the design data.

The weighted average values of the collection efficiency and the ratio absorbed, as represented by equations (22a)-(24a) and (22b)-(24b), respectively, would ideally be obtained from an integration process as shown in these equations. In actuality, the integration has been replaced by an addition process over 50 nm wide wavelength intervals, as outlined in section II of the first semi-annual report.

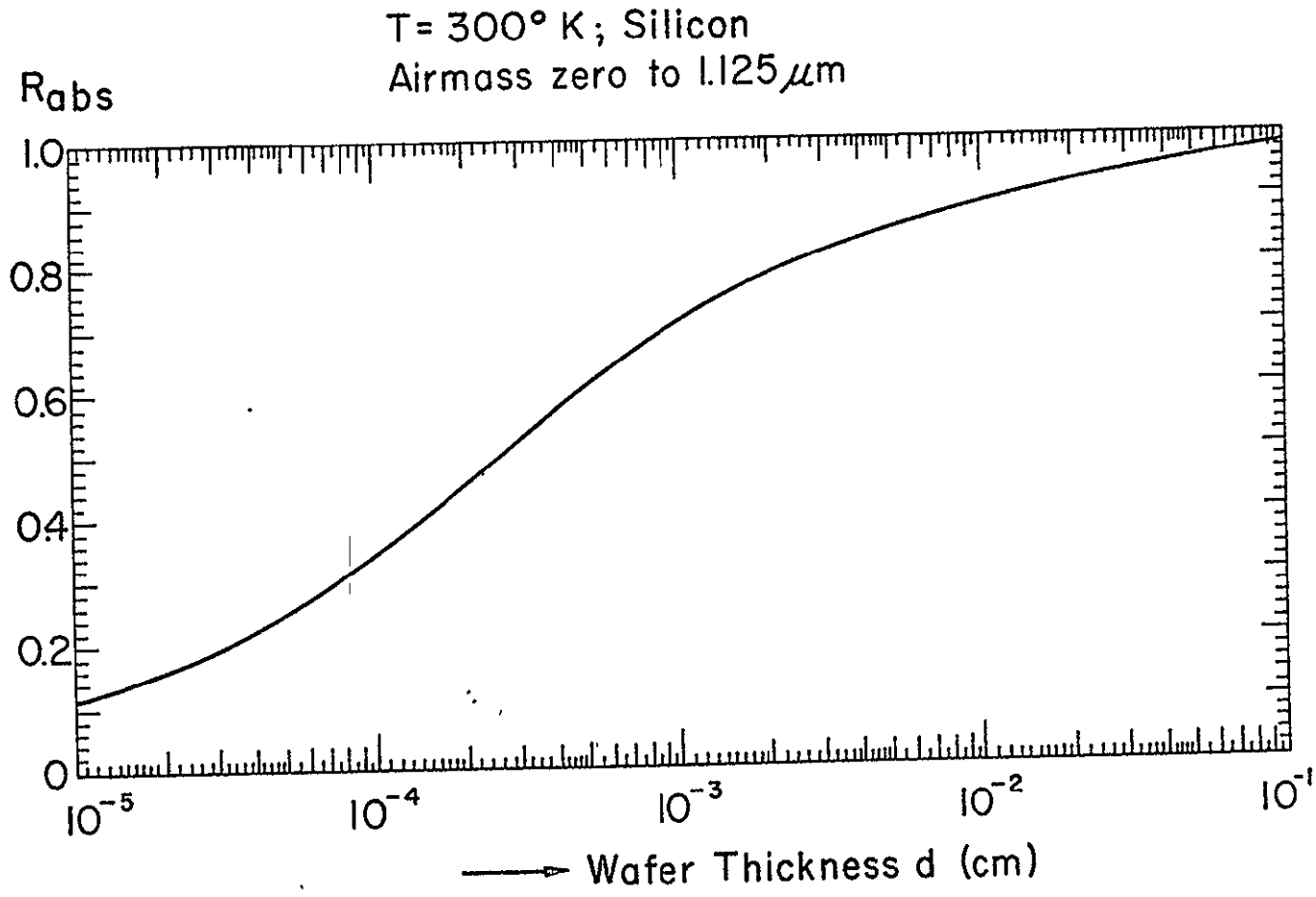

Fig. II - 1 Ratio R_{abs} of the number of photons absorbed in a single pass through a silicon layer of thickness d to the number entering the layer, as contained in airmass zero sunlight up to 1.125 μm wavelength.

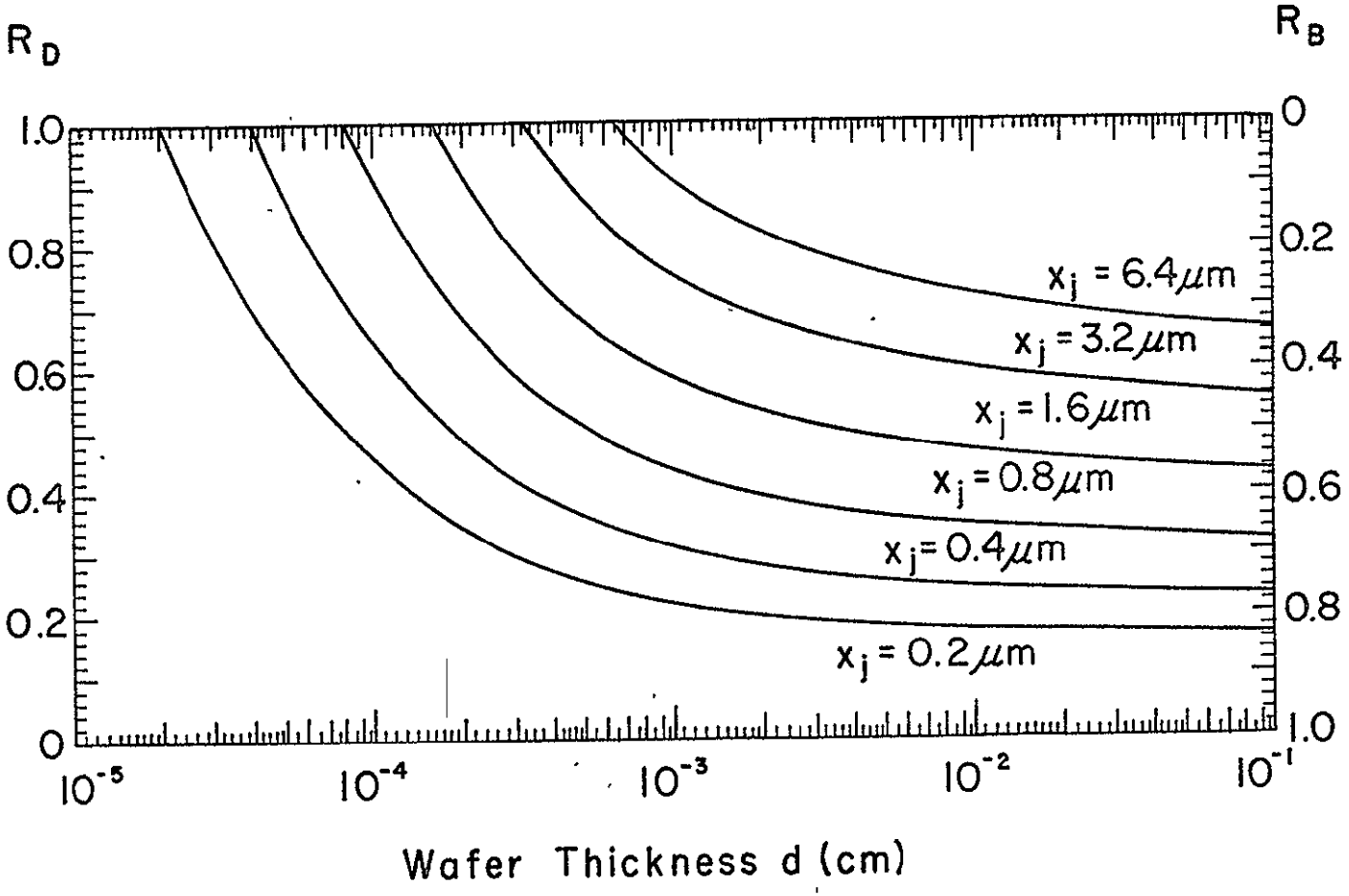

II-2 Ratios R_D and R_B of the number of photons of airmass zero sunlight which are absorbed in the diffused region and the base region, respectively, as function of wafer thickness d. The ratio is taken relative to the number of photons absorbed in the wafer of thickness d, and is presented parametically for various thicknesses x_j of the diffused region (depletion region width zero). Where the depletion region width is not zero, $x_{T,P}$ and $x_{T,B}$ will be used for the diffused region and the base region, respectively.

The determination of the weighted average collection efficiency requires a knowledge of the collection efficiency as function of wavelength, that is $\eta(\lambda)$. These functions $\eta(\lambda)$ have been calculated by use of the computer program SOCEL2, which was discussed in section II of the first semi-annual report. This program is based on an exact solution of the continuity equation for minority carriers. The only basic assumption entering into this differential equation is related to the recombination statistics and is contained in the concept of minority carrier lifetime to be independent of the concentration of the carriers or the way in which they are produced. This is related to the fundamental assumption of small signal theory, that conditions never deviate substantially from thermal equilibrium conditions. This entails, for instance, that the injected carrier density never significantly changes the majority carrier concentration.

An additional, more restrictive assumption has been made to obtain analytical solutions from the continuity equation. This assumption requires the independence of the material constants from the space coordinate x. In those cases where no impurity density gradient exists within a region, this assumption is fulfilled. However, in general, it is not fulfilled in the diffused region. It is also not fulfilled in any subregion where a drift field is purposely introduced. Here, the minority carrier lifetime τ and mobility μ will be functions of x. The drift field E depends on the impurity density distribution with x. E is independent of x, if this impurity density distribution has an exponential dependence on x.

The method used by this author was to assume constant material parameters τ and μ, approximately equal to the weighted average value for the region. Thus, the larger part of the region has material constants of slightly pessimistic value, while a smaller part uses a slightly optimistic value.

As mentioned, constancy of the drift field E requires either a constant or an exponential impurity distribution. Complementary error function distributions are more likely to be encountered. However, an approximation of this distribution by

an exponential function is reasonably close for the major part of the distribution, and thus the assumption of constant drift field is frequently not a bad one.

This author has found earlier (ref.2) that the same performance can be obtained from the diffused region either by minority carrier diffusion only, with a certain diffusion length, or by drift and diffusion combined, with a shorter diffusion length and an electric field corresponding to the expected impurity diffusion profile. Since neither electric field nor diffusion length are measured directly, but are inferred from the performance, this author has preferred to use the simpler case of no field and longer diffusion length. Once more is known about the actual diffusion profiles, the design curves should be reviewed. In the meantime, they form good approximations.

In the same paper (ref.2), this author used the same method used here to investigate the influence of a drift field in the base region on cell performance under the influence of damaging nuclear particle radiation. The drift field was used in a subregion near the pn-junction. Several other authors have since attempted to improve on this method by analyzing the same problem. The authors of ref.3 have included a linear dependence of μ, τ, and E on x in the first subregion of the base. However, they considered the second subregion in the base as a passive layer, that is, not contributing any carriers to the collection process. The effect of this assumption is to move the optimum to greater subregion 1 thickness, and to make the analysis not equivalent to that of ref.2. They further assumed the base region to be infinitely thick and thus could neglect any effect of surface recombination velocity on the back surface.

The authors of ref.4 went to much greater pain in utilizing the known dependence of lifetime and mobility on impurity concentration, and in using an electric field distribution corresponding to the complementary error function distribution of the impurities. Also, they do not appear to have made the assumption of non-collection from the subregion behind the drift field region. These authors found that there is "only a slight reduction of collection efficiency in going from the exponential case to the complementary error function case, if the width of the drift field

in the exponential case is taken to be equal to the thickness of the epitaxial layer" which essentially means to exclude the high concentration portion of the complementary error function distribution. In general, the results of ref.4 appear to be extremely close to those obtained in ref.2 by the "constant field and material parameter" assumption. More recently, another pair of authors (ref.5) has dealt with the same subject, primarily trying to reconcile the differences between references 3 and 4. However, their approach is also questionable since they neglected generation of electrons in the base subregion behind the drift field region. Further, use of the boundary condition of continuity of n and $\frac{dn}{dx}$ at the subregion interface expresses the physical requirement of continuity of minority carrier flow across this interface only, if the drift field at this interface is zero on both sides of the interface. However, ref.5 treats cases where this condition is not fulfilled. Here, the boundary conditions of ref.2 would have been required. Despite these discrepencies, the results of their computations indicate, that the assumptions of constant material parameters and constant drift field do not substantially alter the dependence of short circuit current or collection efficiency on the physical parameters studied. Moreover, they show that the constancy assumption even leads to the proper quantitative values, if judicious choice of the constant values is made. Analysis of the data shows that despite all the differences in assumptions between ref.2 to ref.5, the quantitive results do not appear to differ by more than 3 to 5 percent in comparable cases, and these differences are probably at least partially caused by differences in the mobility versus impurity concentration data used.

Another question occasionally raised concerns the integration over wavelength. Ref.3 to ref.5 have followed Kleinman's approach (ref.6) of integrating first over wavelength, thus obtaining a non-analytical forcing function in dependence on x for entry into the ordinary, linear, inhomogeneous differential equation. This author solved the differential equation analytically with constant coefficients for discrete wavelength values in the range of interest, and added the solutions to obtain the total light generated current. The latter method has the advantage that

$j(\lambda)$ and $\eta(\lambda)$ are obtained, that is the spectral response. This permits more detailed comparison with experiment. While analytical solutions are not available with non-constant coefficients, the numerical methods could still be applied to obtain spectral response data.

Both methods, that is integration over wavelength either before or after solution of the differential equation, are mathematically equally valid. In either case, the integration, due to the non-analytical nature of $N_{ph}(\lambda)$, has to be replaced by a summation with adequately fine steps. Thus, the forcing function is a sum. Since we deal with an ordinary, linear differential equation, the solution of the inhomogeneous equation is the sum of the general solution of the homogeneous equation and a particular solution of the inhomogeneous equation. Since the forcing function is a sum, the particular solution of the inhomogeneous equation can be expressed as a sum of the particular solutions for each of the addends of the forcing function. This is the principle of the "spectral response" approach. Both approaches, if properly executed should yield the same results.

To summarize the discussion on the limitations of the data used:

1. The data relating to homogeneous subregions are accurate.
2. Where subregions with drift fields have been analyzed, an approximation has been used. From results obtained by other methods, it may be concluded that:
   a. The relationships between various design parameters and performance have been obtained in very close approximation.
   b. Absolute values of collection efficiency may be off by a few percent, depending primarily on the choice of material parameters, such as mobility, made.

After this preamble, then, the design curves for collection efficiency from the diffused region and the base region are presented in the following. The meaning and impact of various design approaches have been discussed in the first semi-annual report, and the curves are rather self-explanatory, so that further discussions at this point should not be necessary. The data presented previously have been augmented

by new collection efficiency curves for the base region for diffused region thickness of 0.8, 2.5, and 6.4 μm, to complete the set of design parameters covered and to round out the visibility of impact of variation of the individual parameters. With increasing thickness of the diffused region, the light generated current contribution from the base region decreases rapidly, but the collection efficiency from both the diffused and the base regions decrease also.

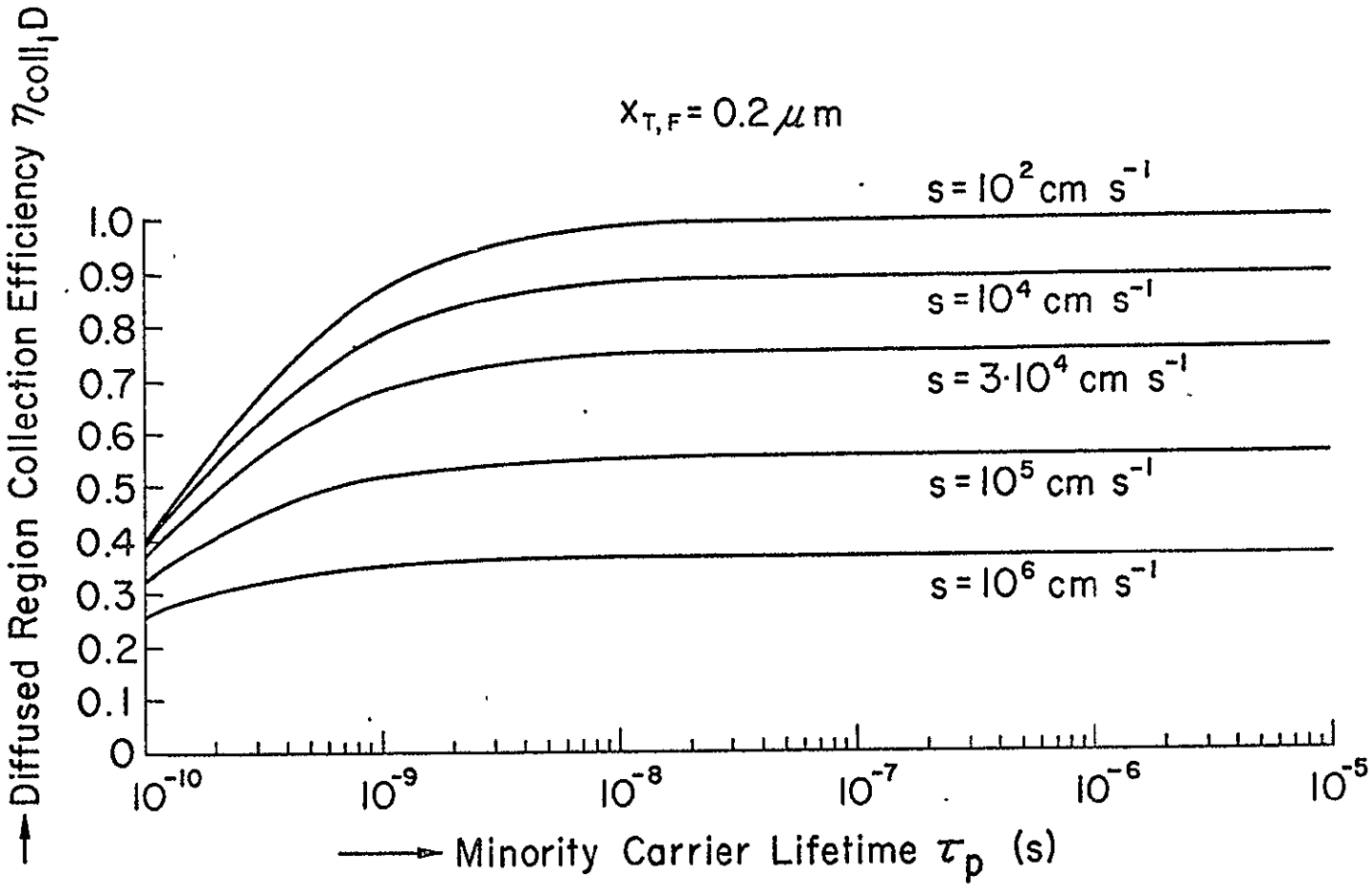

Fig. II - 3 Collection Efficiency $\eta_{coll,D}$ from the diffused region as function of minority carrier lifetime, for several values of surface recombination velocity s. (Diffused region thickness $x_{T,F} = 0.2\,\mu m$.)

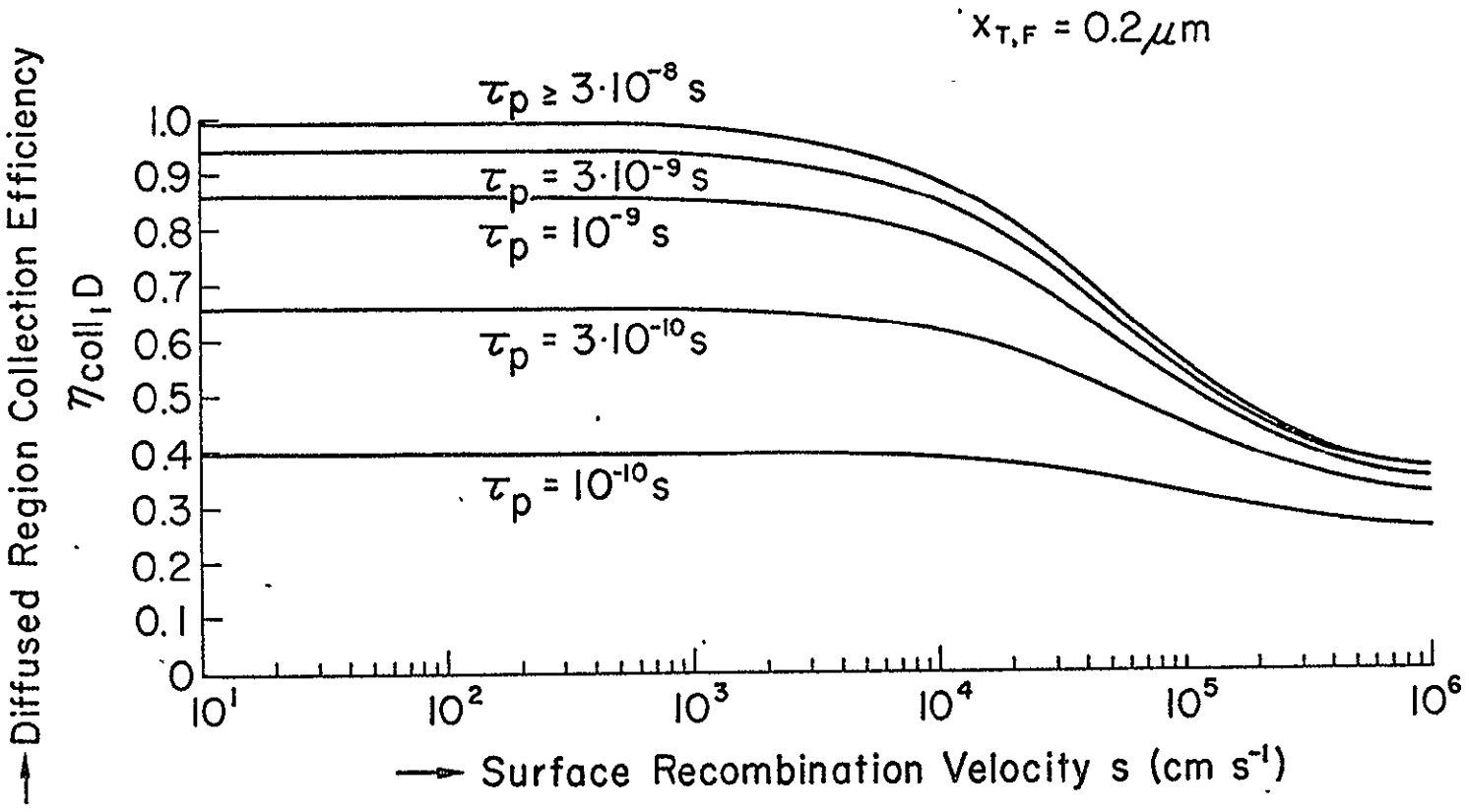

Fig. II-4 Collection Efficiency $\eta_{coll,D}$ from the diffused region as function of surface recombination velocity, for several values of minority carrier lifetime τ_p. (Diffused region thickness $x_{T,F} = 0.2\,\mu m$.)

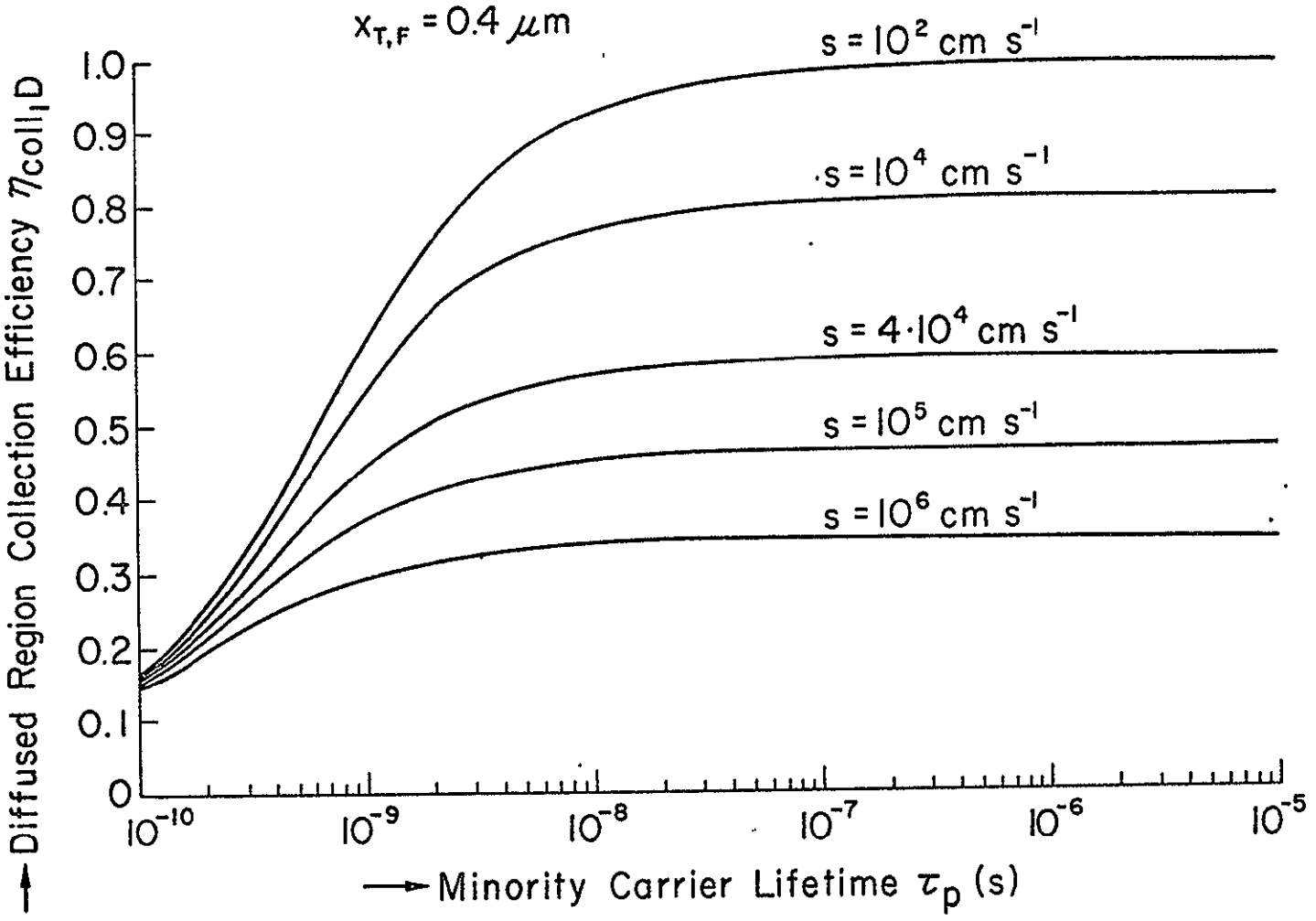

Fig. II - 5 Collection efficiency $\eta_{coll,D}$ from the diffused region as function of minority carrier lifetime, for several values of surface recombination velocity s, (Diffused region thickness $x_{T,F} = 0.4\mu m$).

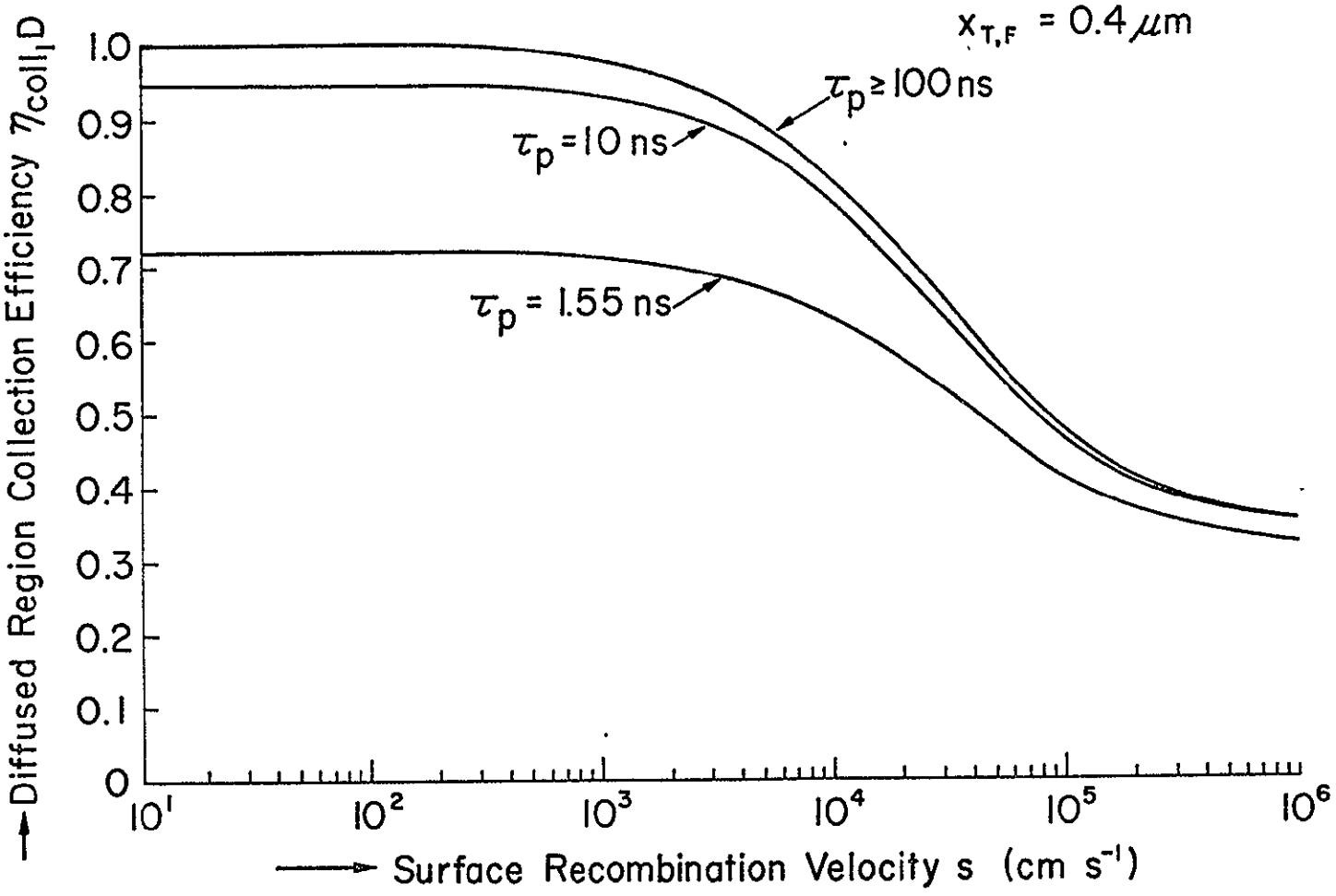

Fig. II - 6 Collection efficiency $\eta_{coll,D}$ from the diffused region as function of surface recombination velocity, for several values of minority carrier lifetime τ_p. (Diffused region thickness $X_{T,F} = 0.4\mu m$)

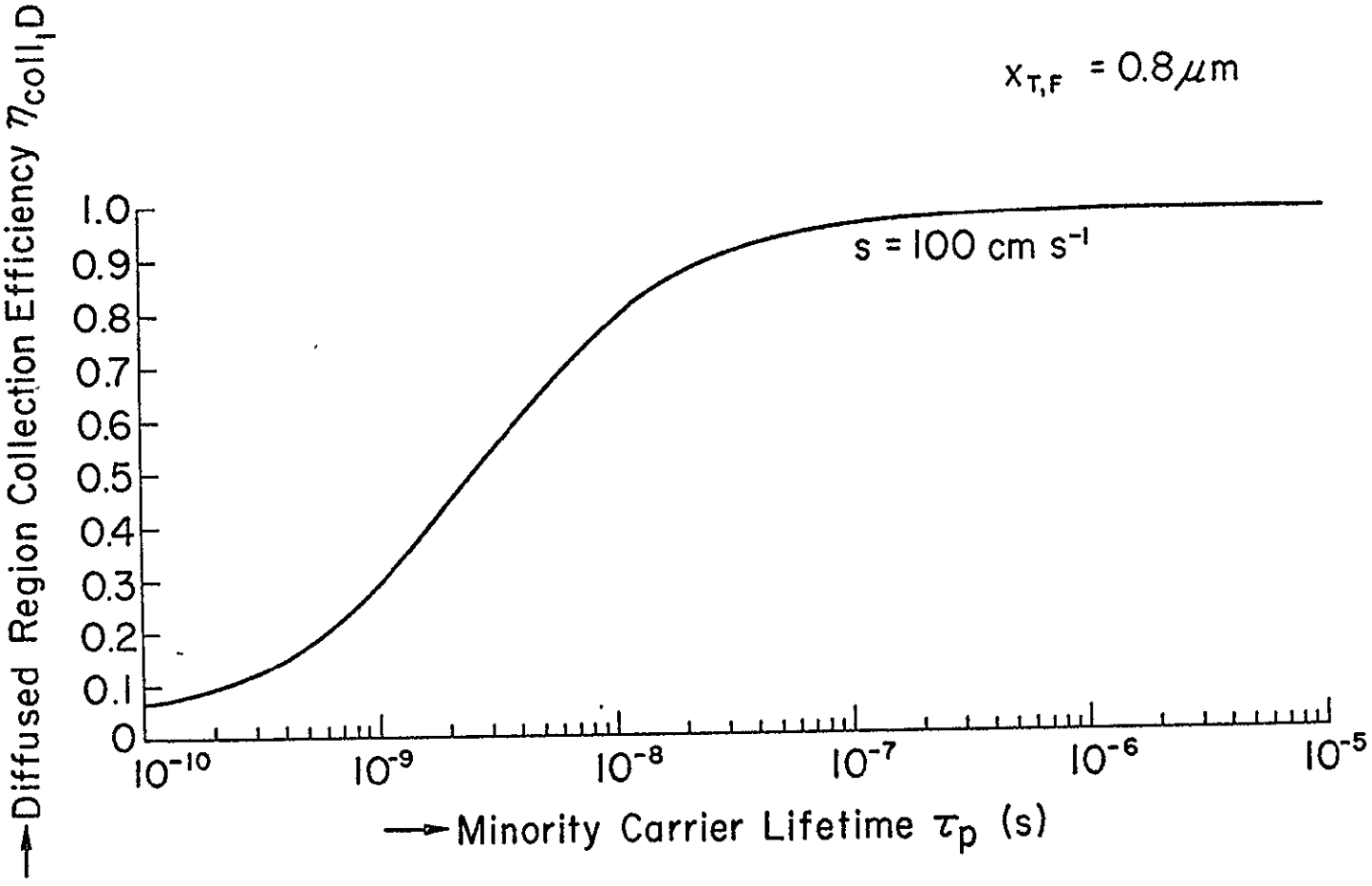

Fig. II-7 Collection Efficiency $\eta_{coll,D}$ from the diffused region as function of minority carrier lifetime, for a diffused region thickness $x_{T,F} = 0.8\mu m$.

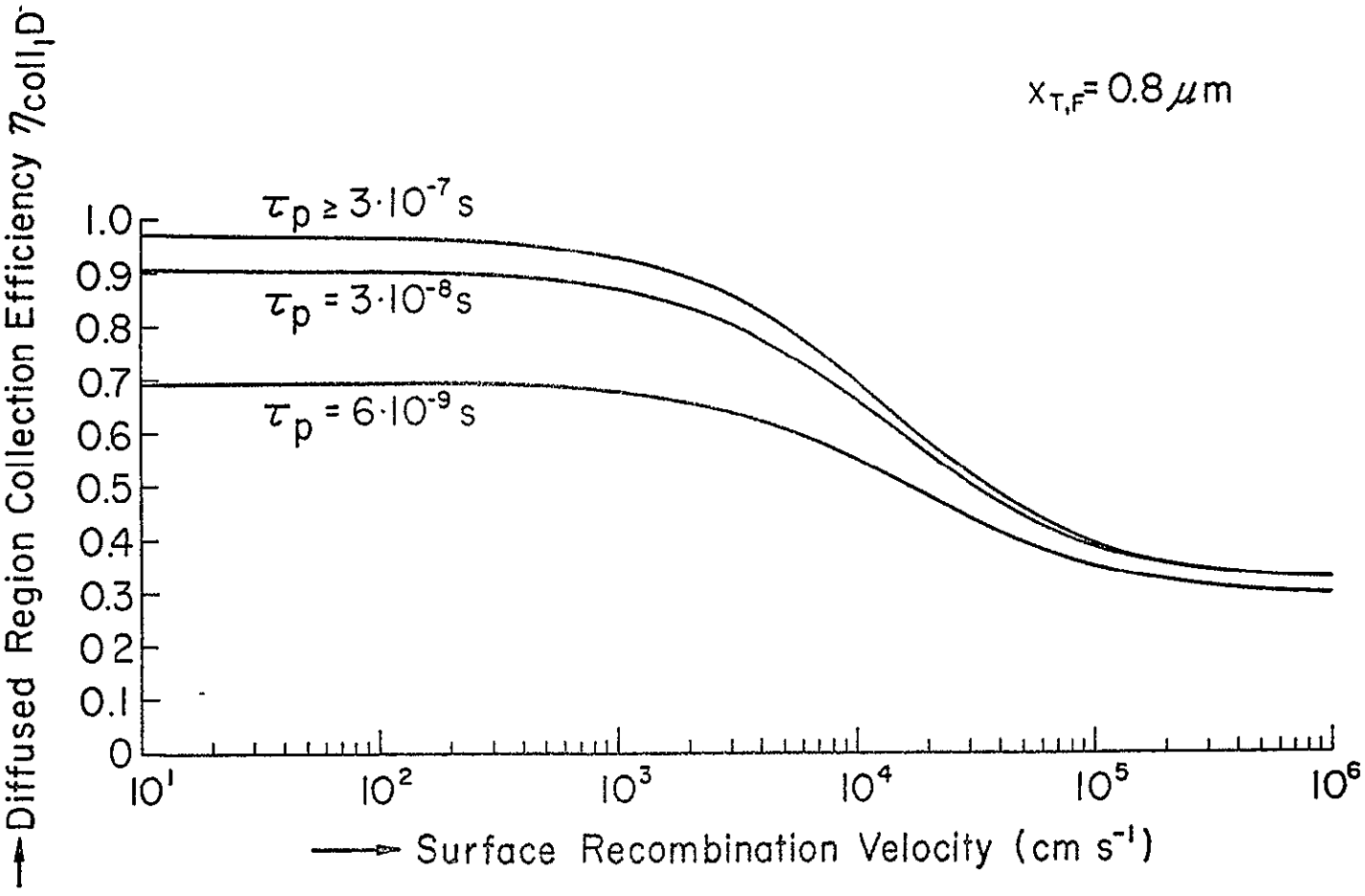

Fig. II-8 Collection Efficiency $\eta_{coll,D}$ from the diffused region as function of surface recombination velocity, for several values of minority carrier lifetime τ_p. (Diffused region thickness $x_{T,F} = 0.8\,\mu m$.)

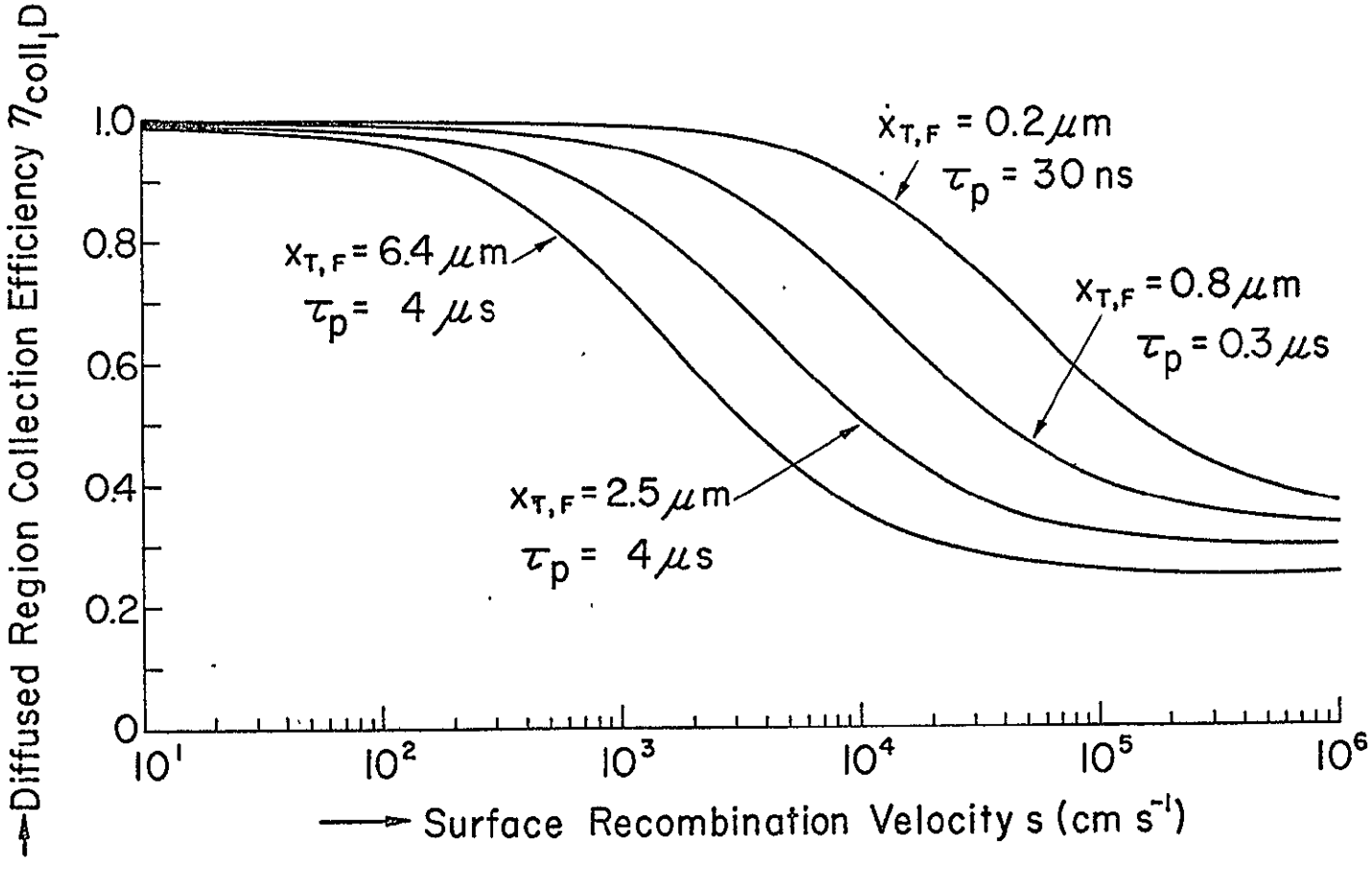

Fig. II - 9 Collection efficiency $\eta_{coll,D}$ from the diffused region as function of surface recombination velocity, for several values of diffused region thickness $x_{T,F}$ with minority carrier lifetime values τ_p which yield maximum light generated current.

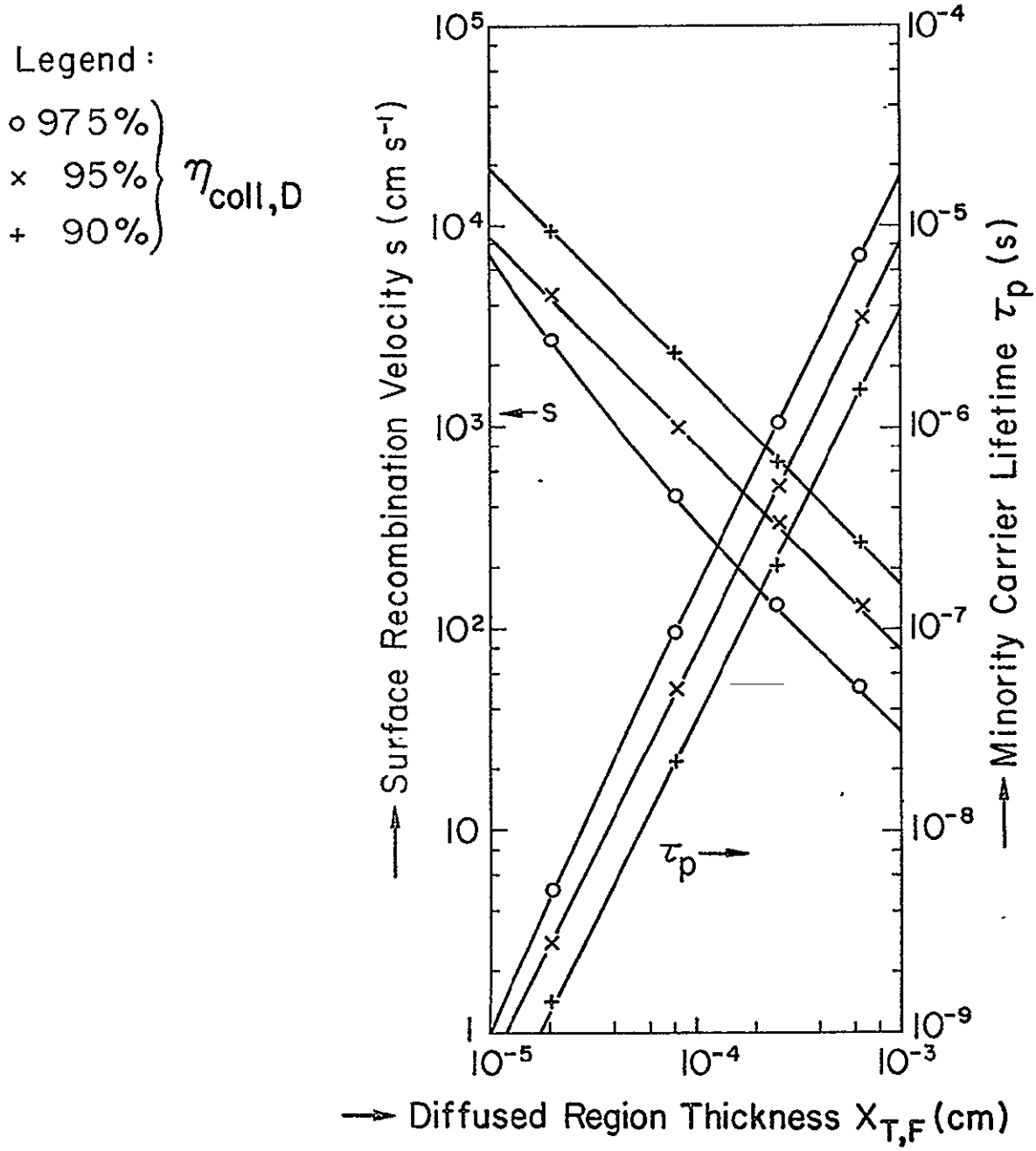

Fig. II - 10 Design curves for the material parameters as function of the diffused region thickness. The curves yield the values of minority carrier lifetime and surface recombination velocity s, for which a collection efficiency of 97.5%, 95%, and 90%, respectively, can be obtained, assuming the other one of these 2 parameters being adjusted so that this is possible.

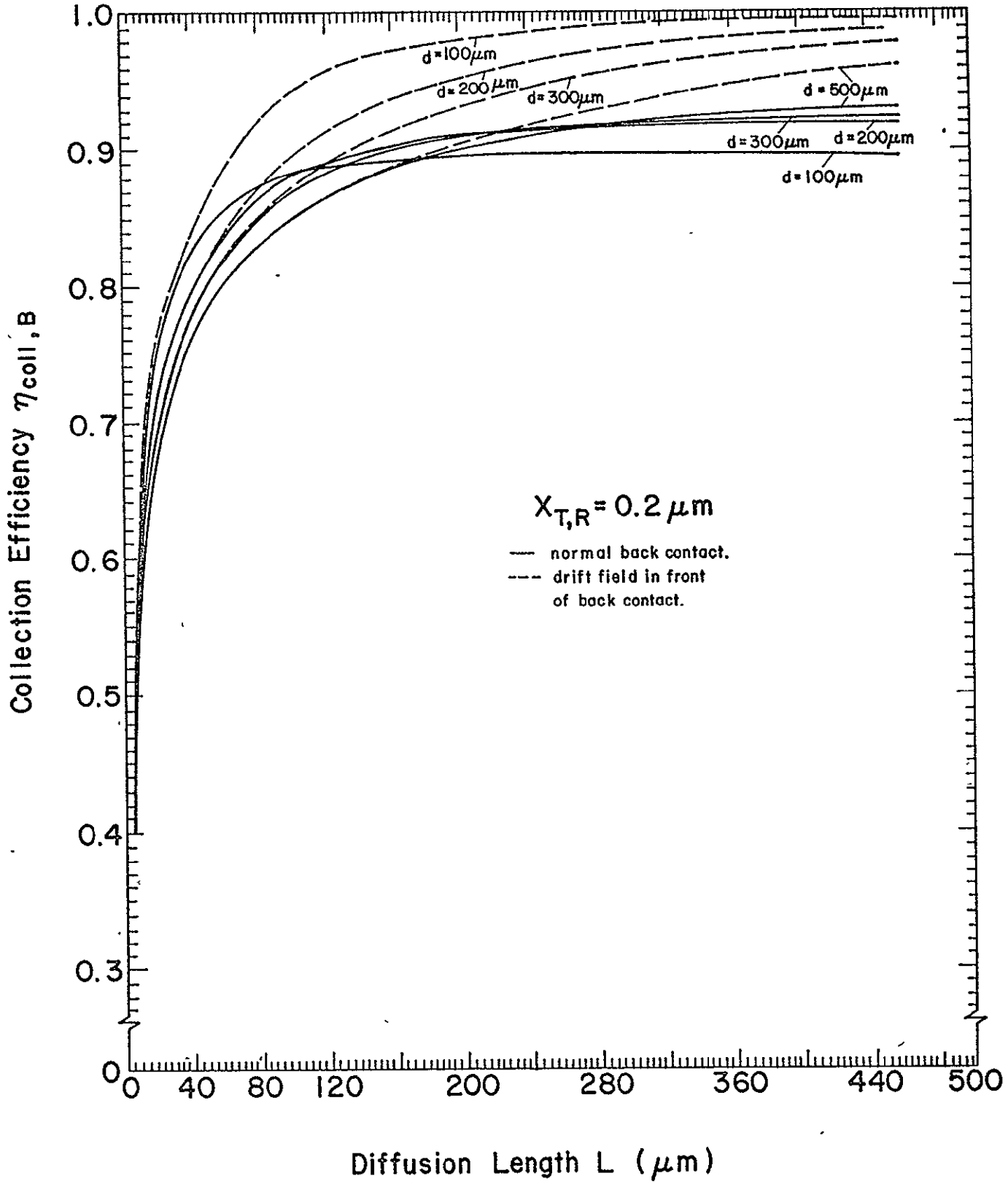

Fig. II - 11 Collection efficiency $\eta_{coll,B}$ from the base region as function of diffusion length for 3 values of thickness for silicon solar cells in airmass zero sunlight. $x_{T,R} = 0.2\,\mu m$.

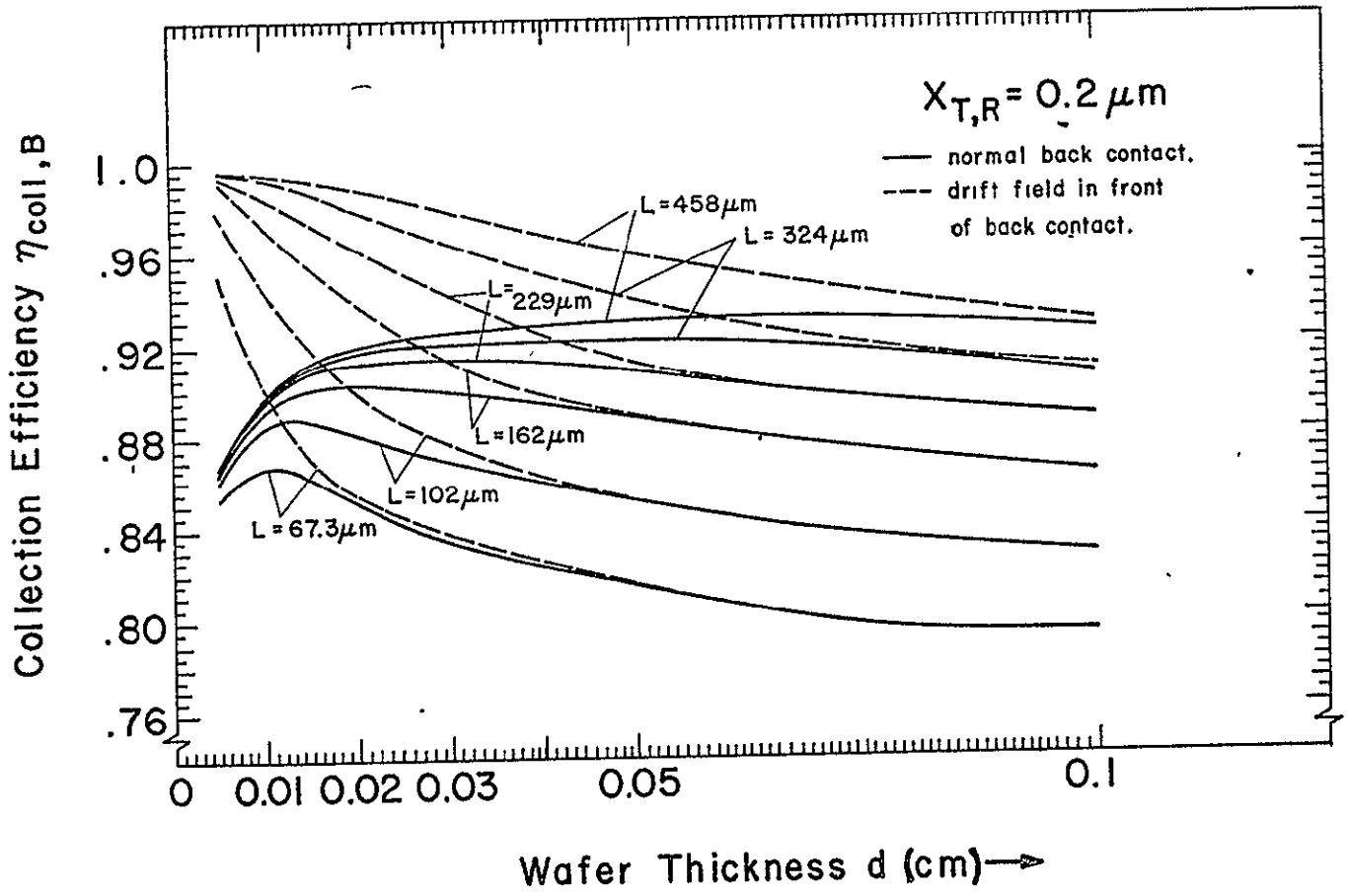

Fig. II-12 Collection Efficiency $\eta_{coll,B}$ from the base region as function of wafer thickness d, for 3 values of diffusion length in the base region, with and without a drift field in front of the back contact. Airmass zero sunlight, T = 300° K. × $_{T,R}$ = 0.2 μm.

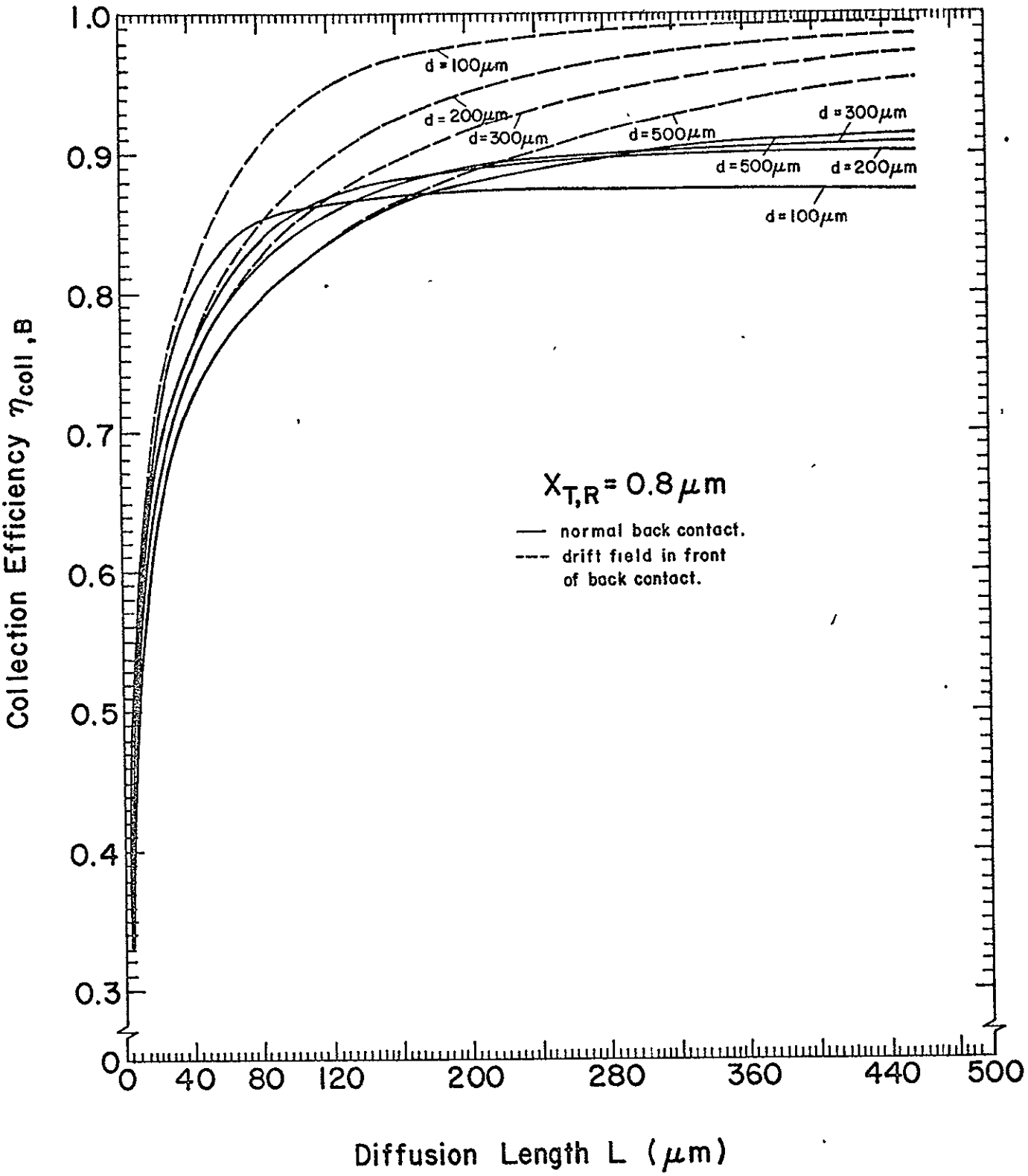

Fig. II - 13 Collection Efficiency $\eta_{coll,B}$ from the base region as function of diffusion length for 3 values of thickness for silicon solar cells in airmass zero sunlight. $x_{T,R} = 0.8\,\mu m$.

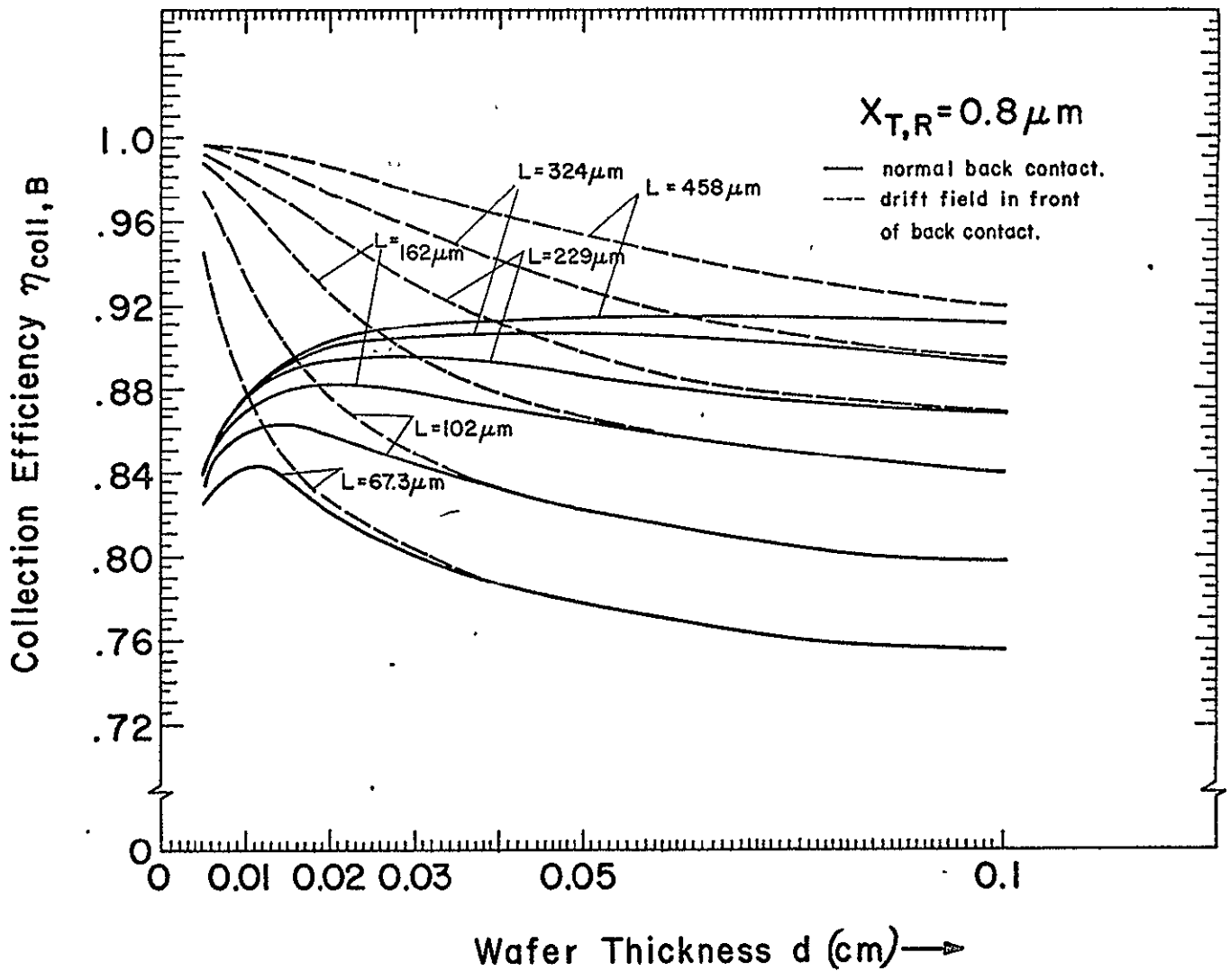

Fig. II-14 Collection Efficiency $\eta_{coll,B}$ from the base region as function of wafer thickness d, for 3 values of diffusion length in the base region, with and without a drift field in front of the back contact. Airmass zero sunlight, T = 300° K. $x_{T,R} = 0.8\,\mu m$.

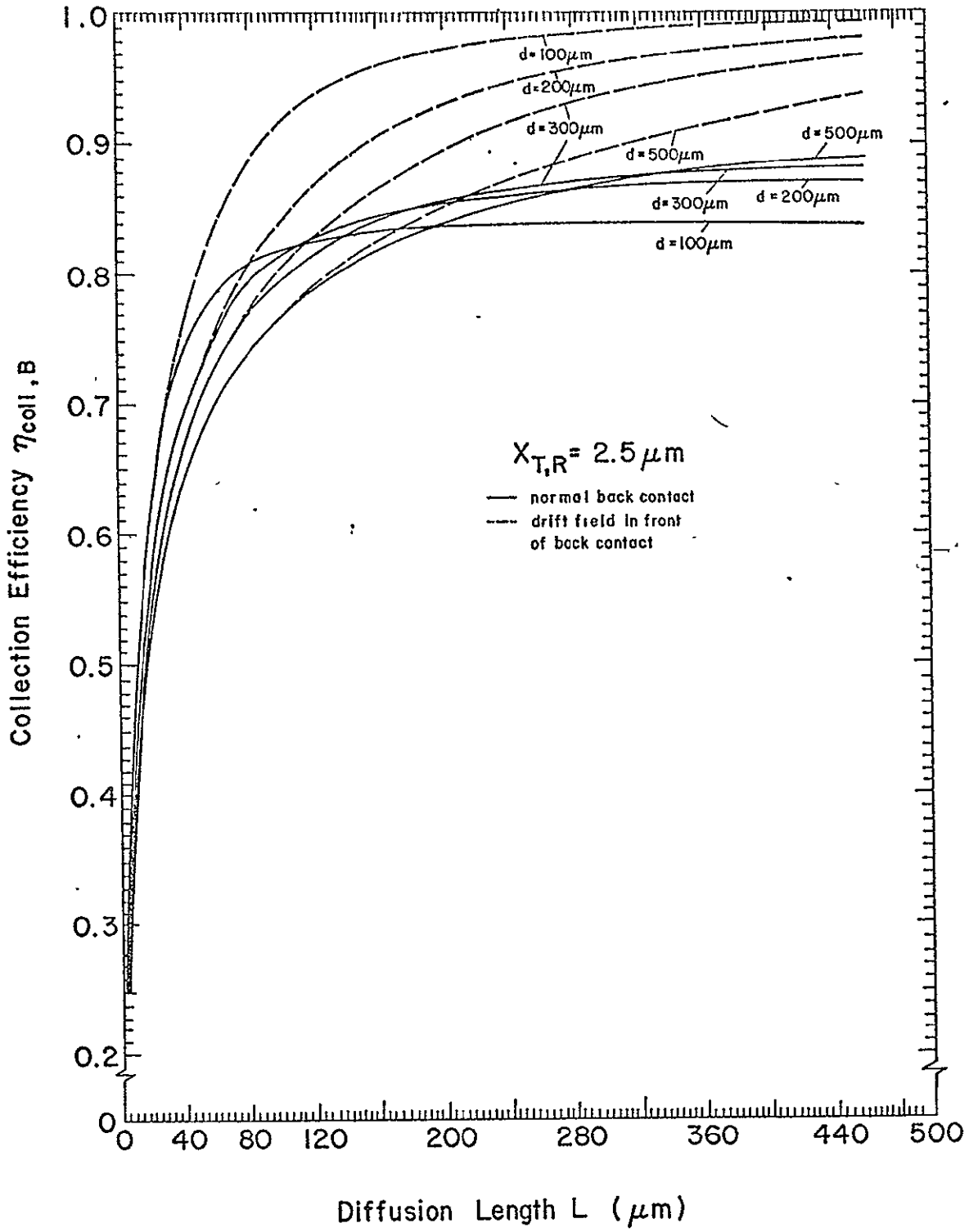

Fig. II - 15 . Collection Efficiency $\eta_{coll,B}$ from the base region as function of diffusion length for 3 values of thickness for silicon solar cells in airmass zero sunlight. $x_{T,R} = 2.5 \mu m$.

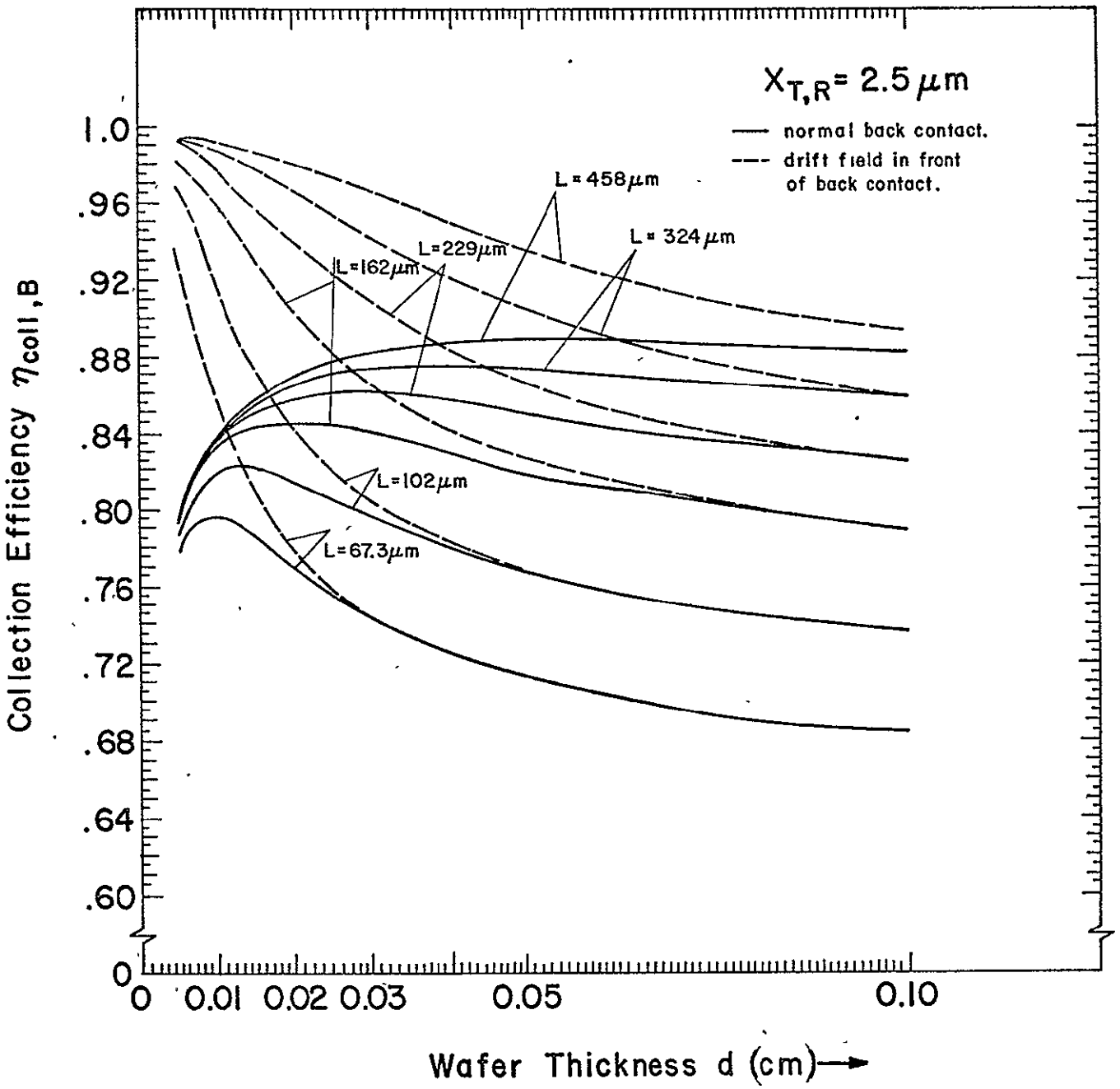

Fig. II-16 Collection Efficiency $\eta_{coll,B}$ from the base region as function of wafer thickness d, for 3 values of diffusion length in the base region, with and without a drift field in front of the back contact. Airmass zero sunlight, T = 300° K. $x_{T,R}$ = 2.5 μm.

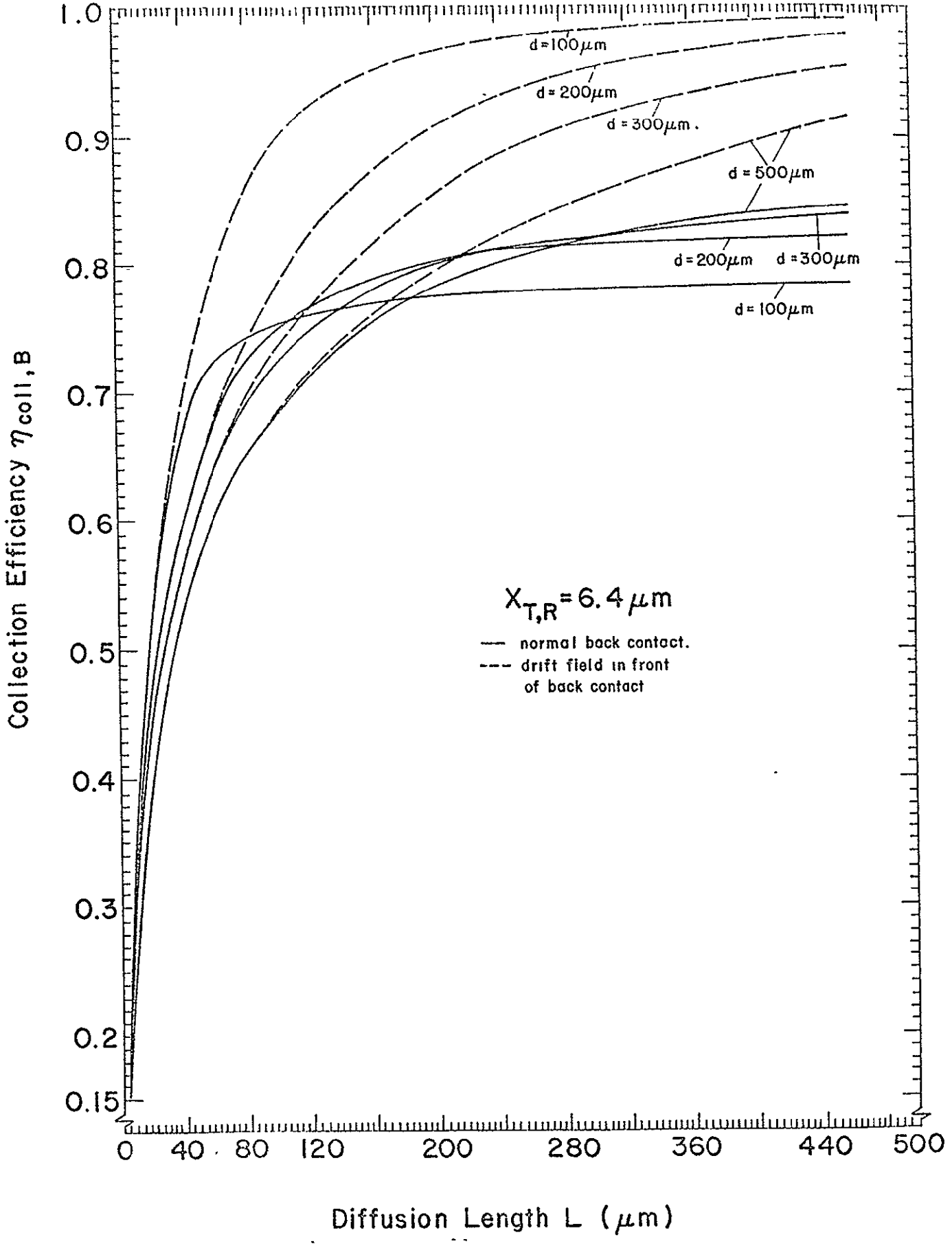

Fig. II-17 Collection Efficiency $\eta_{coll,B}$ from the base region as function of diffusion length for 3 values of thickness for silicon solar cells in airmass zero sunlight. $x_{T,R} = 6.4\ \mu m$.

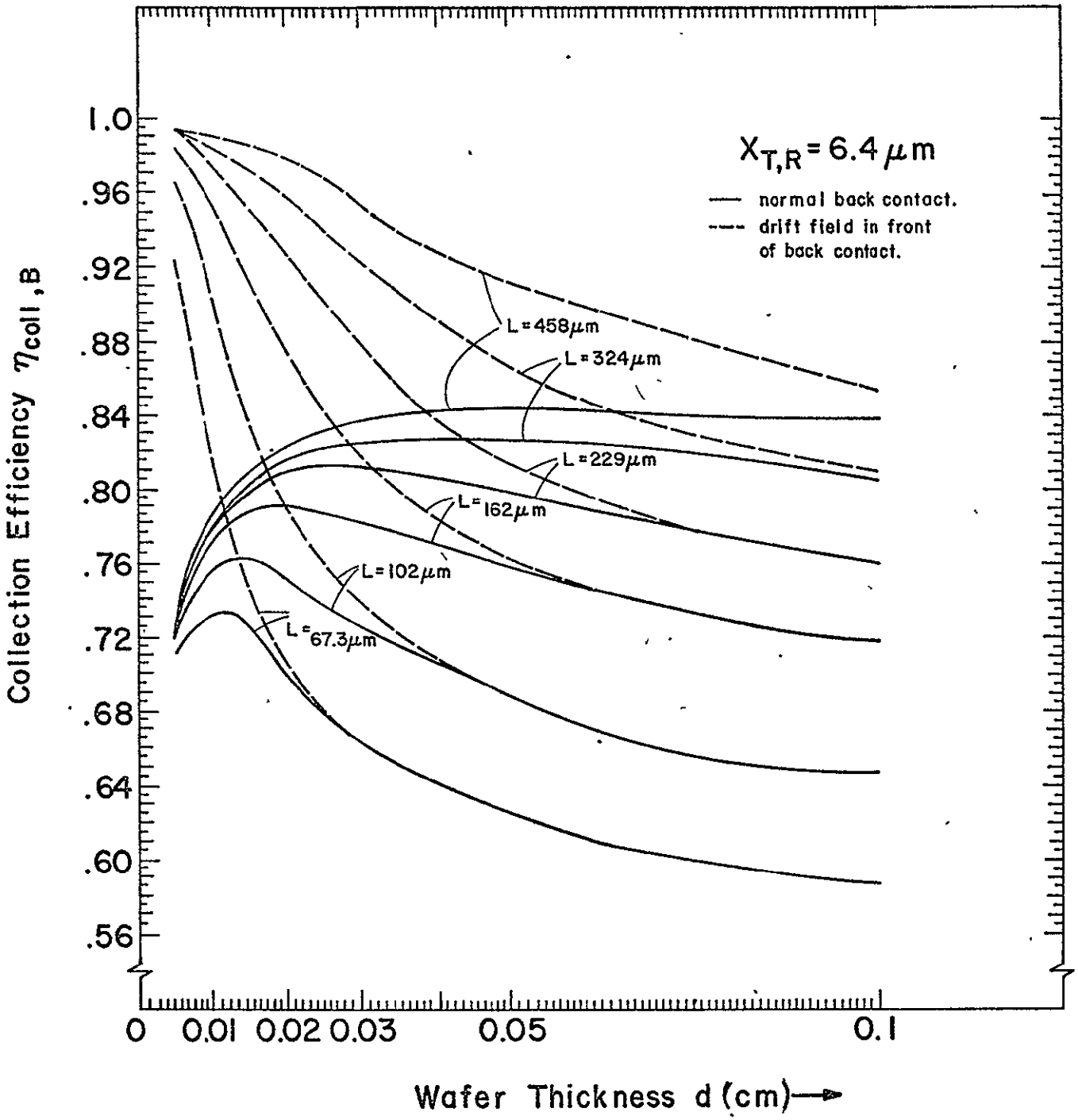

Fig. II - 18 Collection Efficiency $\eta_{coll,B}$ from the base region as function of wafer thickness d, for 3 values of diffusion length in the base region, with and without a drift field in front of the back contact. Airmass zero sunlight, T = 300° K. $x_{T,R} = 6.4\,\mu m$.

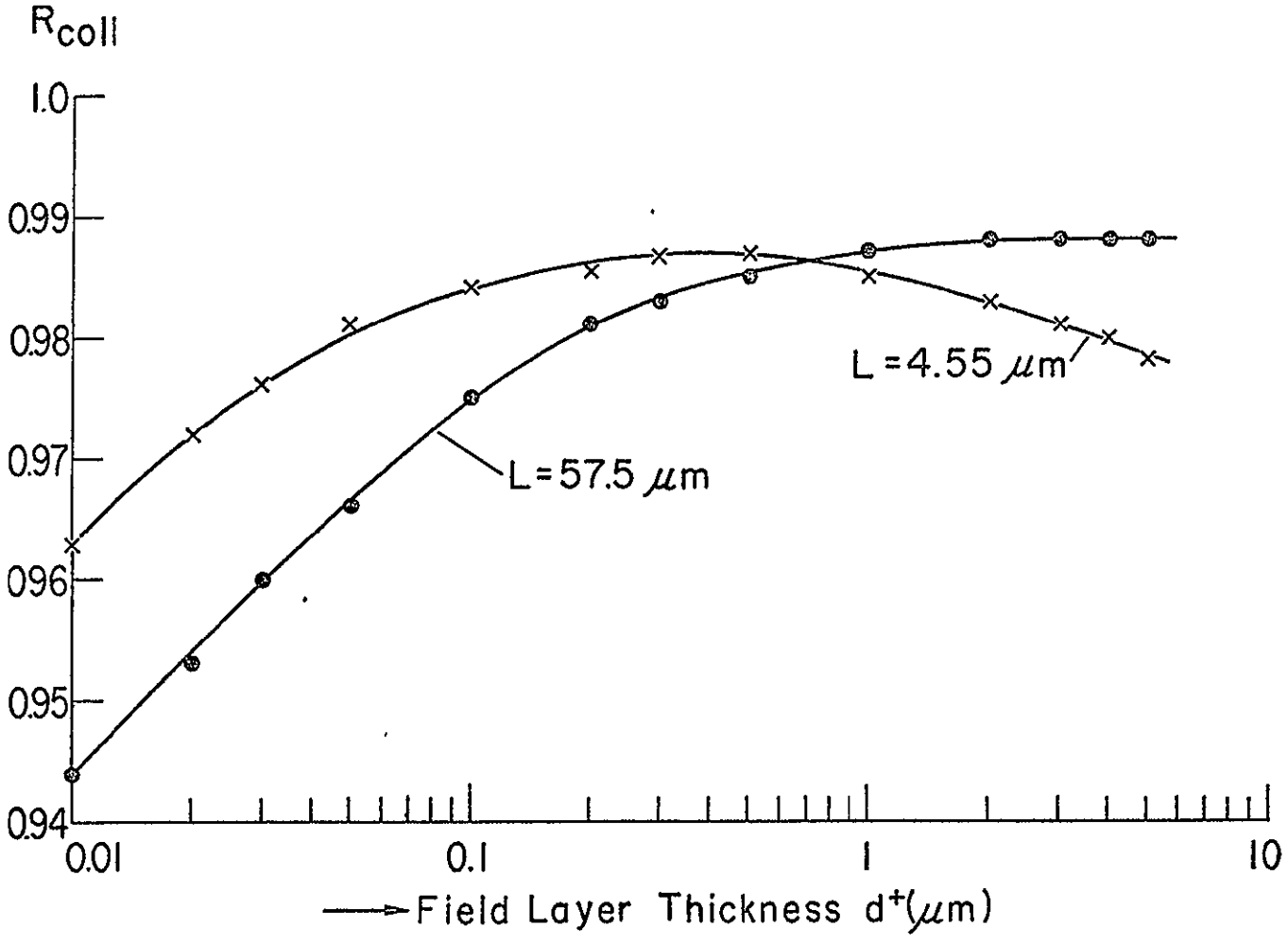

Fig. II - 19 Collection efficiency $\eta_{coll,B}$ from the base region as function of thickness of the drift field layer in front of the back contact for 2 values of mean diffusion length in the drift field layer, for an impurity concentration ratio of 10^4 between p^+ region and base region. $X_{T,R} = 0.2\,\mu m$.

References, Section II:

1. M. Wolf, "Limitations and Possibilities for the Improvement of Photovoltaic Solar Energy Converters. Part I: Considerations for Earth Surface Operation." Proc. IRE 48, pp.1246-1263, July 1960.

2. M. Wolf, "Drift Fields in Photovoltaic Solar Energy Converter Cells," Proc. IEEE 51, pp.674-693, May 1963.

3. S. Kaye and G.P. Rolik, "Optimum Bulk Drift-Field Thickness in Solar Cells," IEEE Trans. ED 13, pp.563-570, July 1966.

4. W.M. Bullis and W.R. Runyan, "Influence of Mobility and Lifetime Variations on Drift-Field Effects in Silicon-Junction Devices," IEEE Trans. ED 14, pp.75-81, Feb. 1967.

5. R. Van Overstraeten and W. Nuyts, "Theoretical Investigation of the Efficiency of Drift-Field Solar Cells," IEEE Trans. ED 16, pp. 632-641, July 1969.

6. D.A. Kleinman, "Considerations on the Solar Cell," Bell Syst. Tech. J. 40, pp.85-115, Jan.1961.

Just as the light generated current can be expressed as a sum of several current contributions from different regions of the solar cell, so can the junction current be expressed as a sum of several current contributions. In the most general case, the contributions do not only originate from different regions of the diode, but can also be based on various mechanisms.

Thus, let:

$$j_d = j_{d,D} + j_{d,T} + j_{d,B} ;$$

where the second subscripts refer to the diffused, transition and base regions, respectively. The most basic mechanism leading to dark diode current is the diffusion current, described extensively by Shockley.[1] At least in the diffused region, it is necessary to take account of the surface recombination velocity. Lindmeyer and Wrigley[2] have discussed the case of the narrow base diode with an ohmic contact covering the entire surface parallel to the pn junction, that is, a surface of practically infinite recombination velocity. The solar cell is more complicated: the width of the diffused region is, in current cells, not small compared to the diffusion length, although in ultimate good cells this should be the case. At present, the surface recombination velocity is high everywhere, but in ultimate good cells, this should be the case only under the ohmic contact strip and the grid lines.

Thus, a more detailed theory is needed, but based on the same principles as used by the above cited references. Of concern is the continuity equation for excess minority carriers: $\hat{p} = p - p_o$ with p_o assumed to be constant:

$$\frac{\partial \hat{p}}{\partial t} = -\frac{\hat{p}}{\tau} + D_p \frac{\partial^2 p}{\partial x^2} = 0 ; \qquad \text{(III-1)}$$

p is the total, instantaneous minority carrier concentration, p_o that which is established in thermal equilibrium conditions. p may be larger or smaller than p_o, with excess carriers recombining or being generated, respectively, with time constant τ. The continuity equation is equal to zero for the steady state case, to be considered here. The general solution for the differential equation is:

$$\hat{p} = p_1 e^{\frac{x}{L_p}} + p_2 e^{\frac{-x}{L_p}} ;$$

with $L_p^2 = \tau D_p$; (III-2)

Using the boundary conditions for the diffused layer:

$$-D_p \left.\frac{\partial \hat{p}}{\partial x}\right|_{x=o} = -s\ \hat{p}\ (0)\ ; \qquad \text{(III-3a)}$$

$$p\ (x_j) = \bar{p}\ ; \qquad \text{(III-3b)}$$

$$-\frac{D_p}{L_p}\ p_1 \quad + \frac{D_p}{L_p}\ p_2 \quad = -s\ p_1 \ - s\ p_2\ ;$$

$$p_1 e^{\frac{x_j}{L_p}} + p_2 e^{-\frac{x_j}{L_p}} = \bar{p}\ ;$$

This leads to the matrix:

$$\begin{pmatrix} p_1 & p_2 & 1 \\ -\left(\frac{D_p}{L_p} - s\right) & \frac{D_p}{L_p} + s & 0 \\ e^{\frac{x_j}{L_p}} & e^{-\frac{x_j}{L_p}} & \bar{p} \end{pmatrix} \qquad \text{(III-4)}$$

and the solution of the main determinant:

$$-\left(\frac{D_p}{L_p} - s\right) e^{-\frac{x_j}{L_p}} - \left(\frac{D_p}{L_p} + s\right) e^{\frac{x_j}{L_p}} = M\ ; \qquad \text{(III-5)}$$

Finally:

$$p_1 = \frac{-\bar{p}\left(\frac{D_p}{L_p} + s\right)}{M}\ ; \qquad \text{(III-6a)}$$

$$p_2 = \frac{-\bar{p}\left(\frac{D_p}{L_p} - s\right)}{M}\ ; \qquad \text{(III-6b)}$$

and:

$$\hat{p}\ (x) = \bar{p}\ \frac{\left(\frac{D_p}{L_p} + s\right) e^{\frac{x}{L_p}} + \left(\frac{D_p}{L_p} - s\right) e^{-\frac{x}{L_p}}}{\left(\frac{D_p}{L_p} + s\right) e^{\frac{x_j}{L_p}} + \left(\frac{D_p}{L_p} - s\right) e^{-\frac{x_j}{L_p}}}\ ; \qquad \text{(III-7a)}$$

$$\hat{p}(x) = \hat{p} \; \frac{\frac{D_p}{L_p}\cosh\frac{x}{L_p} + s\sinh\frac{x}{L_p}}{\frac{D_p}{L_p}\cosh\frac{x_j}{L_p} + s\sinh\frac{x_j}{L_p}}\,; \qquad \text{(III-7b)}$$

The current into the transition region is thus:

$$j_{d,D} = -q\, D_p \left.\frac{\partial p}{\partial x}\right|_{x=x_j}\,;$$

$$= -q\,\frac{D_p}{L_p}\,\bar{p}\;\frac{\frac{D_p}{L_p}\sinh\frac{x_j}{L_p} + s\cosh\frac{x_j}{L_p}}{\frac{D_p}{L_p}\cosh\frac{x_j}{L_p} + s\sinh\frac{x_j}{L_p}}\,; \qquad \text{(III-8)}$$

$$\text{or: } j_{d,D} = -q\,\frac{D_p}{L_p}\,\frac{n_i^2}{n_n}\left(e^{\frac{qV}{kT}} - 1\right)\cdot F\,; \qquad \text{(III-9a)}$$

$$\text{where: } F = \frac{\sinh\frac{x_j}{L_p} + \frac{sL_p}{D_p}\cosh\frac{x_j}{L_p}}{\cosh\frac{x_j}{L_p} + \frac{sL_p}{D_p}\sinh\frac{x_j}{L_p}}\,; \qquad \text{(III-9b)}$$

The factor F includes the dependence on layer thickness, while the remainder of the equation is the familiar relationship for the dark diode current from infinitely thick regions. In fact, the factor F becomes 1 for $\frac{x_j}{L_p} \to \infty$.

For $\frac{sL_p}{D_p} \gg 1$, the F becomes $\cosh\frac{x_j}{L_p}$, yielding the expression of Lindmeyer and Wrigley for the narrow base diode. For $\frac{sL_p}{D_p} \ll 1$, on the other hand, the factor F becomes $\tanh\frac{x_j}{L_p}$, which is less than 1 for small values of $\frac{x_j}{L_p}$.

Thus with thin regions and low surface recombination velocity, the diode (or junction) current can actually be reduced below the normally used values. Since reduction of surface recombination velocity has already been found to be a goal from the collection efficiency viewpoint, as well as making $\frac{x_j}{L_p} \ll 1$, it is satisfying to see that the same requirements are also beneficial for improvement of the IV characteristic.

Detail data, as they will be needed for design purposes, of the dependance of this factor F on layer thickness and the ratio of surface recombination velocity to $\frac{D_p}{L_p}$ are given in Fig. III - 1 and III - 2.

It is clear that the ohmic contact areas, including the grid lines, have high effective surface recombination . In present cells which have high surface recombination everywhere, this is not of much significance. In cells with reduced surface recombination velocity and low values of $\frac{x_j}{L_p}$, as needed for high collection effeciency in the short wavelength region, the contact and grid line areas could contribute greatly to the junction current. To avoid this it will become necessary to diffuse deeply below the contact and grid line areas, as illustrated in Fig. III - 3. Since it will generally not be desirable to see a contribution to the junction current from the contact and grid line areas greater than the contribution from the remaining cell surface this will provide a minimum value for the junction depth $x_{j,C}$ under the contact areas. Designers may actually want to use lower contributions than this. The total solar cell junction current contribution from the diffused layer will then be:

$$j_{d,D} = -q \frac{D_p}{L_p} \frac{n_i^2}{n_n} \left(e^{\frac{qV}{kT}} - 1 \right) \left\{ A_S F_S + A_C F_C \right\} ; \qquad \text{(III-10)}$$

where A_S is the area of the open surface of the diffused region and A_C the area covered by contacts and grid lines, including any edge or "wrap around" areas, and where F_S and F_C are the F factors applying to A_S and A_C, respectively. For the designer's convenience, a curve of F_C versus $\frac{x_j}{L_p}$ is included in Fig. III - 1 labelled $\frac{sL_p}{D_p} = \infty$.

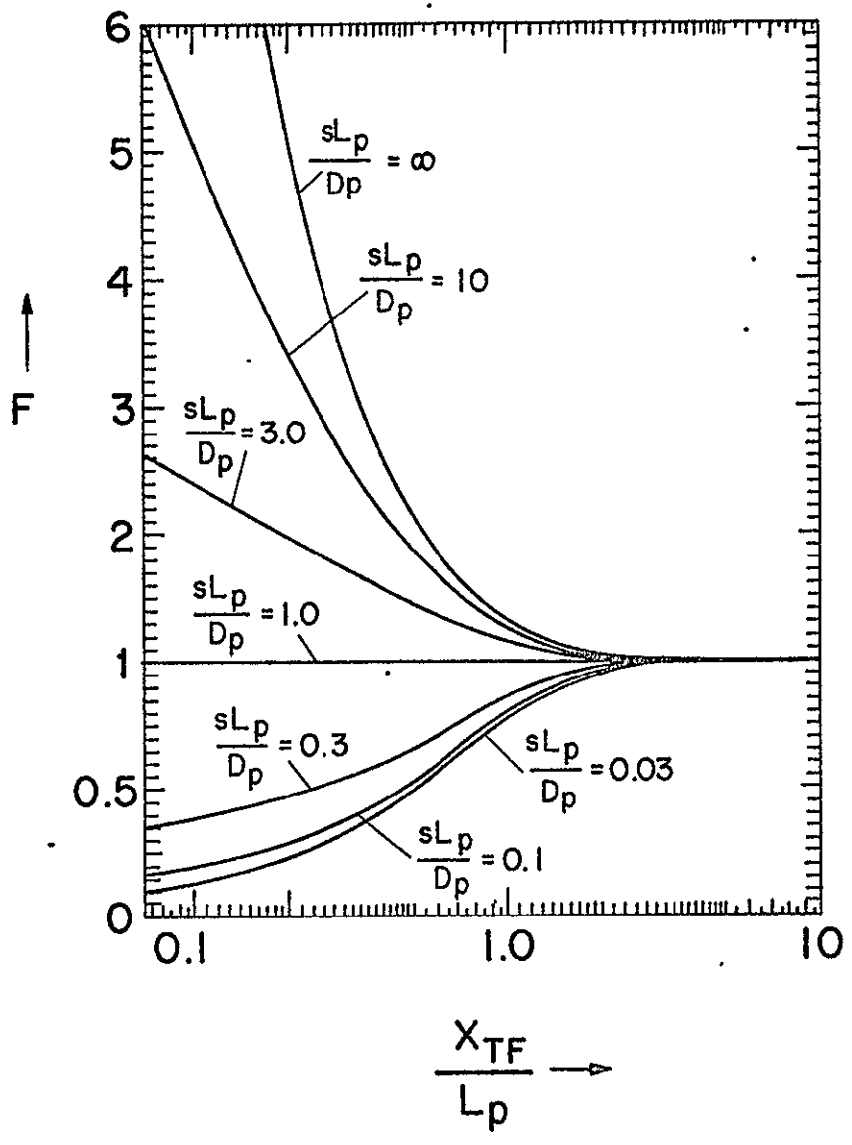

III-1 Form factor F for the dark diode current as function of normalized diffused region thickness $\frac{x_{T,F,}}{L_p}$ with normalized surface recombination velocity $\frac{sL_p}{D_p}$ as parameter.

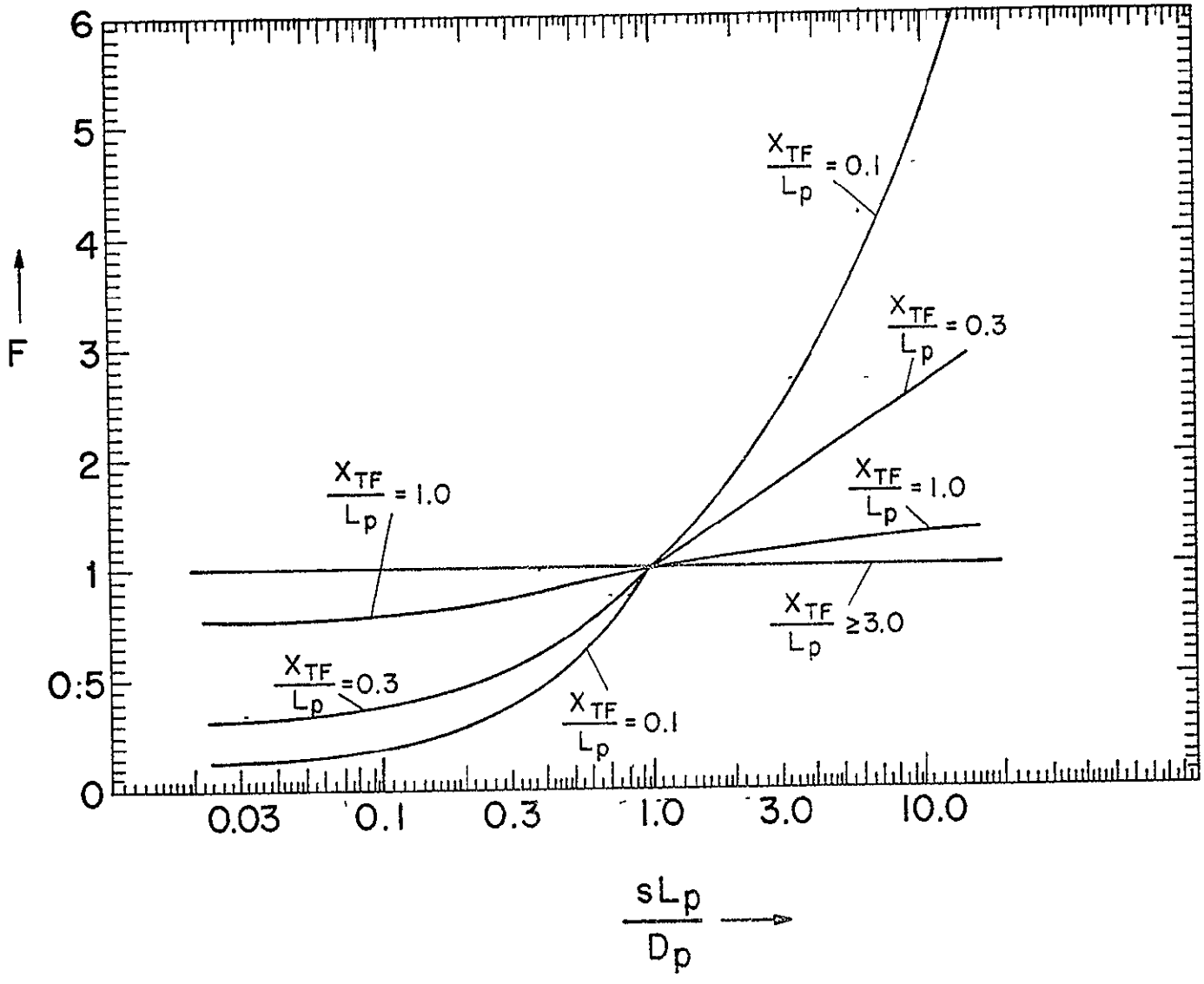

III-2 Form factor F for the dark diode current as function of normalized surface recombination velocity $\frac{sL_p}{D_p}$, with normalized diffused region thickness $\frac{x_{T,F}}{L_p}$ as parameter.

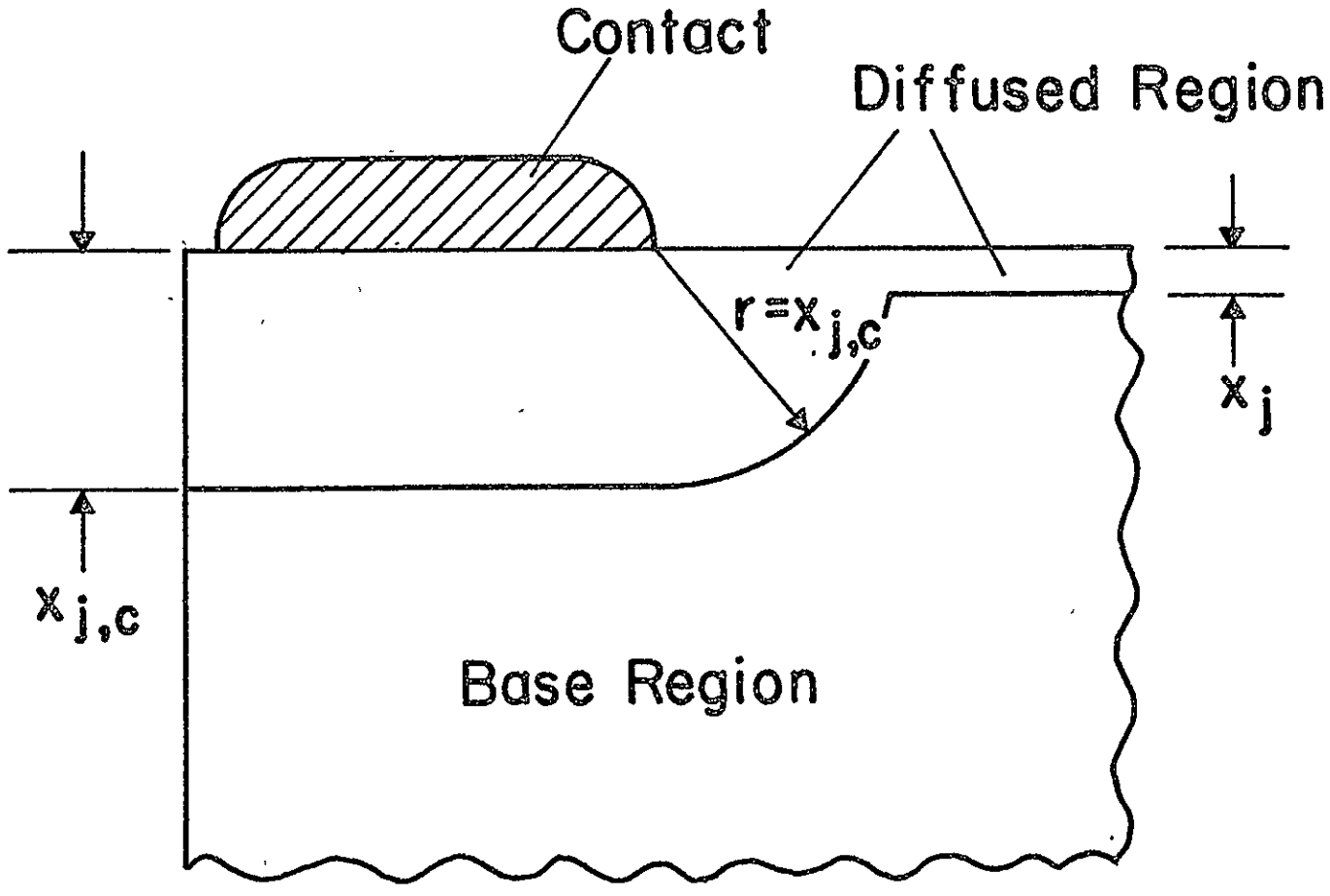
Contact
Diffused Region
$r=x_{j,c}$
x_j
$x_{j,c}$
Base Region

Example:

If for collection efficiency reasons, $\frac{x_j}{L_p} = 0.1$ is chosen, with

$s = 1000$ cm/s, $D_p = 1 \frac{cm^2}{V_s}$ and $L_p = 3.10^{-4}$ cm ($\tau = 9\text{-}10^{-8}$ s), then F_S will be 0.38. If A_C is 10% of the total junction area, then F_C should not exceed 3.4, requiring $x_{j,C} \geq 0.3\ L_p$ under the contacts. For $s = 100$ cm s^{-1}, the corresponding situation leads to $\frac{x_j}{p}, C\ L_p$.

It is thus seen that the deep diffusion requirement is not very severe for many cases which prove adequate from the collection efficiency viewpoint. It is recognized tnat it will be necessary to extend the deep diffusion sideways by an equal distance $x_{j,C}$ in order to realize the full effect on the junction current contributions.

This deep diffused region, not covered by contact metal and thus exposed to incident light radiation, has a lower collection efficiency than the shallow diffused regions. Including grid lines, this exposed deep diffused area may comprise as much as 5% of the exposed cell area, resulting in a 1% decrease in light generated current from the cell if the collection efficiency is reduced by 20% in the deep diffused regions.

Since the single layer model for the dark diode current treated so far is not really representative of the 2 - layer model, including drift fields, used for the collection efficiency calculations, a corresponding 2 - layer model has been developed for the dark diode current (saturation current). First it was attempted to reduce the collection efficiency equation (equation (33) of ref.3) to the zero light intensity case, but this was not found to be readily and uniquely possible. In consequence, a new equation was derived in complete analogy to the derivation of saturation current in the first part of this section and to that of collection efficiency in ref.3. The new equation was expressed in WATFIV language for ease of evaluation by computer.

Subsequently, a multivariable experiment was run on the computer. Although time

did not permit complete evaluation of the data, it appears that, in general, measures that improve collection efficiency do also reduce the saturation current, and vice versa.

A further description of the derivation and an analysis of the results will be included in the next semi annual report.

REFERENCES, Section III

1. W. Shockley, Bell Syst. Tech. J. 28, 435-489, 1949

2. Jos. Lindmeyer and Ch. Y. Wrigley, "Fundamentals of Semiconductor Devices", von Nostrand, Princeton, N.J., pp. 29-34, 1965

3. M.Wolf, "Drift Fields in Photovoltaic Solar Energy Converter Cells," IEEE Proc. 51, pp.674-693, May 1963.

IV EVALUATION OF EXPERIMENTAL CURRENT-VOLTAGE DATA

1. Introduction

To carry out optimum-design studies relating to the current-voltage characteristic, it is imperative that the physical theory determining this characteristic be understood. This understanding has, at least, to be sufficient to name all physical and material parameters which do actually have influence on the IV characteristic of silicon solar cells, and to express the relationship of these parameters to the IV-characteristic. This understanding does not yet exist, although there are a number of theories on pn-junction behaviour. What is first required is accurate measurement of current-voltage characteristics under various conditions on numerous solar cells, and comparison of the experimental data with the prediction of theory. This section reports on some further work towards this aim.

As discussed in section IV of the previous semi-annual report, the current-voltage characteristic of silicon solar cells is better described by the relationship

$$j = j_{01}\left[\exp\left(\frac{qV_D}{A_1 kT}\right) - 1\right] + j_{02}\left[\exp\left(\frac{qV_D}{A_2 kT}\right) - 1\right] \; ; \quad (IV\text{-}1)$$

(j is used for current density, all other symbols as used before)

than by the more commonly applied one containing only one such exponential term. Because of its mathematical features, this relationship will from here on, be called the "two-exponential IV-characteristic", in contrast to the common form, which may be referred to as the "single exponential IV-characteristic". The following subsection discusses a number of observations made in the interpretation of experimental data of IV characteristics, and provides some useful hints to other workers in this field.

2. On the interpretation of experimental data of IV-characteristics

A few interesting observations have been made during the course of this author's work on the current-voltage characteristics, which may be of considerable benefit to the readers if shared with them. These observations are concerned with the use and interpretation of the experimental data on the current-voltage characteristics of solar cells, and are only in secondary manner connected with the computer program for their evaluation.

Figure IV-1 shows a set of experimental current voltage points (solid dots) in the range above 0.25Volt. The classical approach in the interpretation of such data has been to draw two tangents through the straight line portions of the characteristic, and by determining the slope of these tangents, compute the value of the factors A_1 and A_2 in the exponents of the two-exponential IV characteristics. This author has, for some time, found that this approach generally does not lead to satisfactory results. The superposition of the two exponentials with the thus found A values does not usually represent the experimental points, particularly where they fall into the overlap region between dominance of one of the two exponentials, or into the region where the $-I_{02}$ term has significant influence. To overcome this shortcoming, the author has used a manual iterative method which is illustrated in Fig. IV-1. Here, two straight lines are shown as tangents to the experimental data, labelled A_2=8.46 and A_1=1.24. The exponential term with the latter A value fits to the experimental data in the region above 0.55Volt,

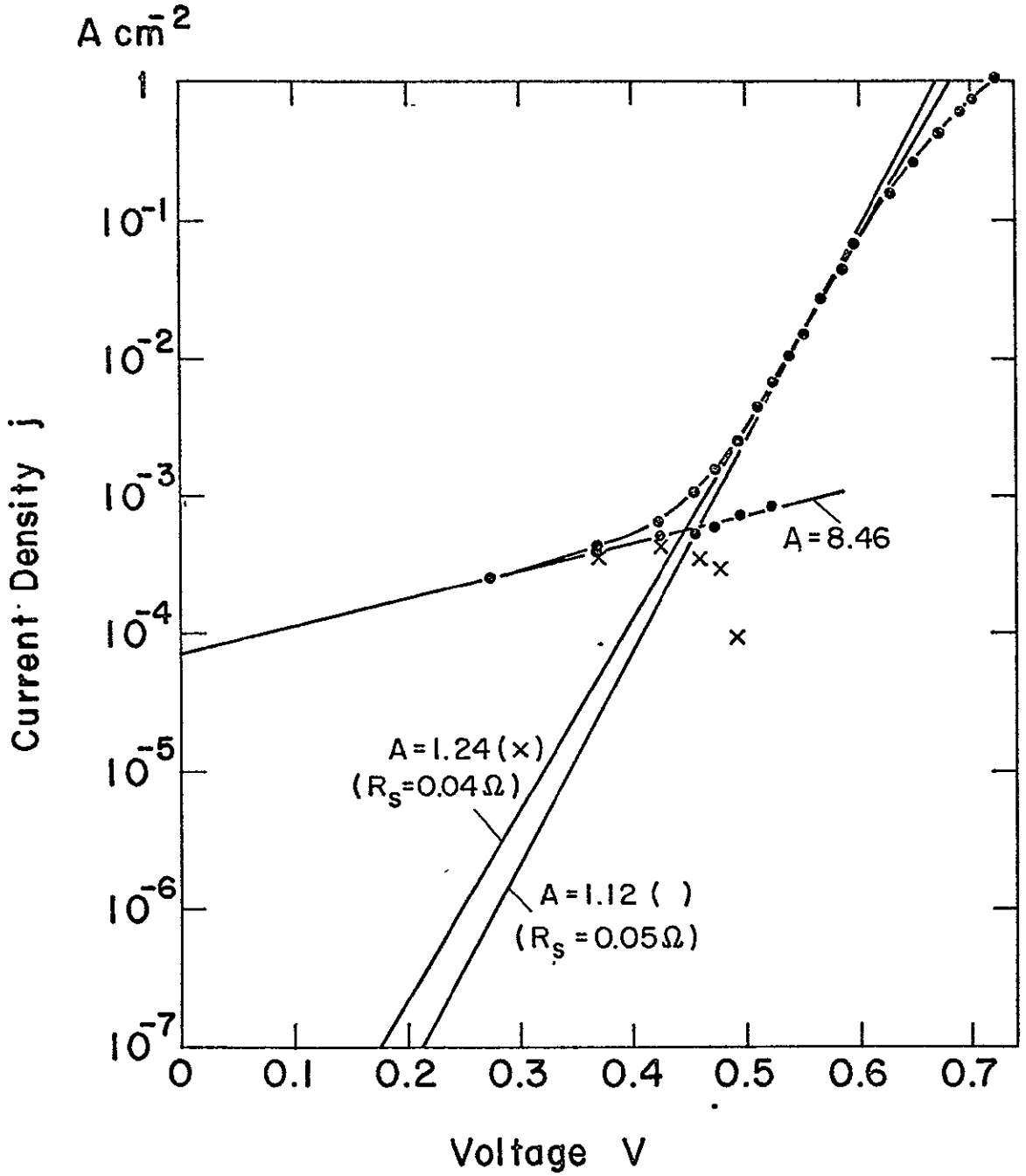

IV-1 Illustration of the superposition of two-exponential term in graphically determining the A-factors from experimental data.

with a series resistance value of .04 Ohm. In the overlap region between the two exponentials, substracting the values of this exponential term from the experimental data points should lead to values represented by the second exponential term containing A_2. The resulting points are indicated by the crosses in Fig. IV-1. It is clearly seen that above 0.4Volt, the two exponential terms discussed so far do not represent the experimental data, since the crosses fall off towards smaller current values at higher voltage, rather than continuing on the straight line representing the exponential term with A_2=8.46. A change in the slope of the exponential with A_1 can remedy this situation as indicated by a second straight line, labelled A_1=1.12 in the semi-logarithmic plot. Subtracting the values of this exponential term from the experimental data points leads to new current values in the region between 0.4 and 0.55Volt. As seen, these values fall nicely onto the straight line of the exponential term with A_2=8.46. Thus, the experimental values can be represented by the superposition of two exponential terms with A_1=1.12 and A_2=8.46, but not by use of an exponential term with A_1=1.24. The latter, however, would have formed a tangent to the upper part of the experimental curve, while the exponential term with the smaller A_1 value intersects the straight line portion of the experimental curve rather than forming a tangent. This observation has been made repeatedly, and will be substantiated with further detail in the following paragraphs.

Figure IV-2 shows the same set of experimental data, this time however, extended to voltages below 0.1Volt. It is seen that the lowest two experimental points fall onto the straight line with slope A_2=8.45. However, an effect of the $-I_{02}$ term would have been expected to be noticeable on these lower points. The extrapolation of the exponential term to its intersect with the ordinate yields the value of I_{02}. Using the value of $7 \cdot 10^{-5}$ Acm^{-2} obtained in Fig. IV-2, and subtracting this value from the experimental data yields the curve represented by crosses. It is seen that this curve differs

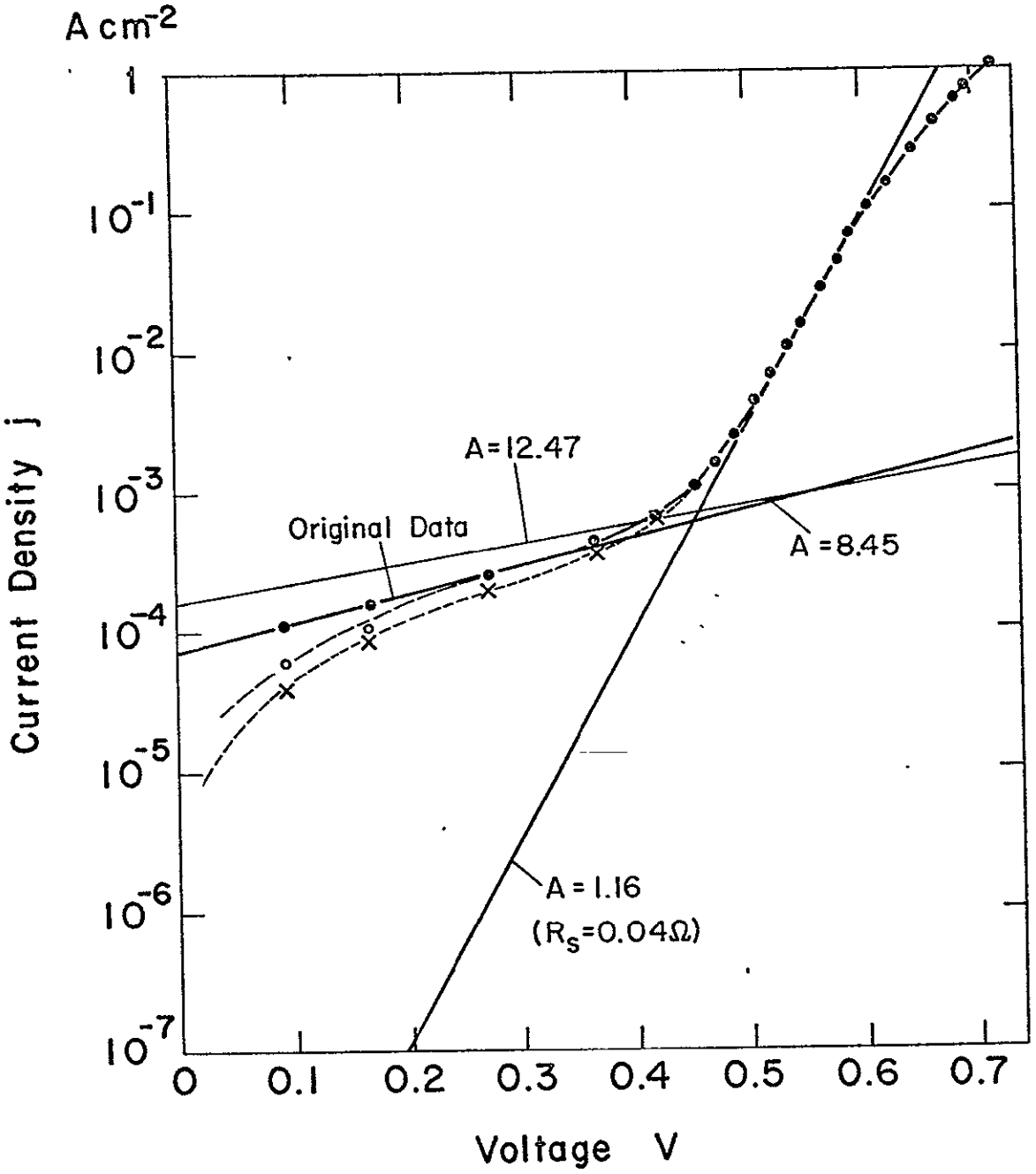

IV-2 Illustration of the influence of the - j_{02} term as the current-voltage characteristic of solar cells.

considerably from the actual experimental data. It is also seen that any attempt to use an exponential term with a smaller slope to explain the experimental data in the region above 0.2Volt, will lead to a larger value of I_{02} and, consequently, to a larger curved part of the resulting characteristic at the lower voltage values. As a compromise, an exponential close to that labelled A_2=12.47 has been chosen, and the resulting saturation current I_{02} has been subtracted from the points on the straight line representing this exponential term in the semilogarithmic plot. The result was a significant deviation from the experimental data only at the two lowest points, as indicated by the hollow circles.

It is interesting to note that the computer program VICHAR was not able to converge with the original experimental data points. It was able, however, to find convergence for the curve composed of the experimental data points (solid dots) above 0.46Volt and of the corrected points marked by crosses, at lower voltages, as well as for the curve given by the experimental data points above 0.2Volt and the hollow circles below.

It was later determined that the experimental data had been faulty. It is very easy to obtain erroneous data points from the instrumentation at such low current values due to inappropriate internal resistance of the measuring equipment, due to noise pick-up, or ground loops. Thus, inability to fit all data points to a theoretical relationship, or large values of standard deviation obtained by use of the computer program VICHAR, or inability to converge may well be caused by faulty experimental data, and should lead to a re-examination of the instrumentation if such occurrances are noted.

In order to further analyze the relationship between the values of the individual exponential terms and the points resulting from their superposition with the inclusion of series resistance, three models of solar cell characteristics were prepared. A second purpose of this undertaking was to check the ability of the computer program to find the actual values which were used to generate such a curve. For Model 1, the values of A_1=1.0, A_2=2.0, $j_{01}=10^{-10}$ A cm^{-2}, and $j_{02}=10^{-6}$ A cm^{-2} were chosen, together, with R=0.5 Ohm,

MODEL 1

Two-Exponential Current-Voltage Characteristic

$I_{01} = 1.10^{-10}$ Acm^{-2}, $A_1 = 1.0$; $I_{02} = 1.10^{-6}$ Acm^{-2}; $A_2 = 2.0$; R = 0.5 Ω

V_D	$I_{01}\exp\left(\frac{qV_D}{A_1 kT}\right)$	$I_{02}\exp\left(\frac{qV_D}{A_2 kT}\right)$	$-I_{02}$	I	V
0.01792		$1.4142 \cdot 10^{-6}$	$-1.0 \cdot 10^{-6}$	$4.142 \cdot 10^{-7}$	
0.03584		2.0	-1.0	$1.0 \cdot 10^{-6}$	
0.08321		5.0	-1.0	4.0	
0.11904		$1.0 \cdot 10^{-5}$	-1.0	9.0	
0.15488	$1.0 \cdot 10^{-8}$	2.0	-1.0	$1.901 \cdot 10^{-5}$	
0.2023	$2.5 \cdot 10^{-7}$	5.0	-1.0	4.925	
0.2381	$1.0 \cdot 10^{-6}$	$1.0 \cdot 10^{-4}$	-1.0	$1.000 \cdot 10^{-4}$	
0.2739	4.0	2.0	-1.0	2.03	0.2740
0.3213	$2.5 \cdot 10^{-5}$	5.0	-1.0	5.24	0.3216
0.3571	$1.0 \cdot 10^{-4}$	$1.0 \cdot 10^{-3}$	-1.0	$1.099 \cdot 10^{-3}$	0.3576
0.3930	4.0	2.0	-1.0	2.399	0.3942
0.4167	$1.0 \cdot 10^{-3}$	3.162	-1.0	4.161	0.4188
0.4346	2.0	4.472	-1.0	6.471	0.4378
0.4583	5.0	7.071	-1.0	1.207	0.4643
0.4762	$1.0 \cdot 10^{-2}$	$1.0 \cdot 10^{-2}$		2.0	0.4862
0.4941	2.0	1.414		3.414	0.5112
0.5178	5.0	2.236		7.236	0.5540
0.5357	$1.0 \cdot 10^{-1}$	3.162		$1.316 \cdot 10^{-1}$	0.6015
0.5536	2.0	4.472		2.447	0.6760
0.5773	5.0	7.071		5.707	0.8627

TABLE IV-1

$T=300^{o}K$. The data for current density were computed to four digit accurracy, and the voltage values were corrected, where appropriate, to reflect the voltage drop across the series resistance, to the same accurracy. The values of the exponential terms themselves, the j_{02} value, their superposition, and the corrected voltage values are shown in Table IV-1. The resulting current-voltage points are plotted as solid dots in Fig. IV-3. The resulting IV characteristic seems to have straight line portions over more than two orders of magnitude in the lower voltage region and of approximately one order of magnitude in the higher voltage region. The tangents to the straight line portions of the resulting IV characteristics are shown as dashed lines. However, the A values for these straight line portions are $A_2=1.87$ and $A_1=1.67$, while the values generating the data were $A_1=1.0$ and $A_2=2.0$. These original exponential terms are represented by solid lines in Fig. IV-3. It is seen that the exponential term containing A_1 is far from being tangent to the straight line portion in the upper part of the characteristic, but, rather intersects it at an angle of approximately 30^{o}. It is also clear that quite a bit of manual iteration would be required to find the appropriate exponential terms to explain the experimental data. This author has frequently spent two or three hours for the manual iteration process on one set of experimental data.

Table IV-2 shows another set of data, called Model 2. The only difference in comparison to Model 1 is a change to $j_{02}= 10^{-7}\ A\,cm^{-2}$. Figure IV-4 presents the corresponding data points, the tangents to the straight line portions of the characteristics, shown by dashed lines having $A_1=1.19$, and $A_2=1.84$, as well as the generating curves with $A_1=1.0$ and $A_2=2.0$. While the table shows the large overlap regions between the various terms in the equation, the figure indicates straight line portions of the characteristic of approximately two orders of magnitude for both the A_1 and the A_2 regions. Again, the generating exponential terms are represented by intersecting lines rather than tangents.

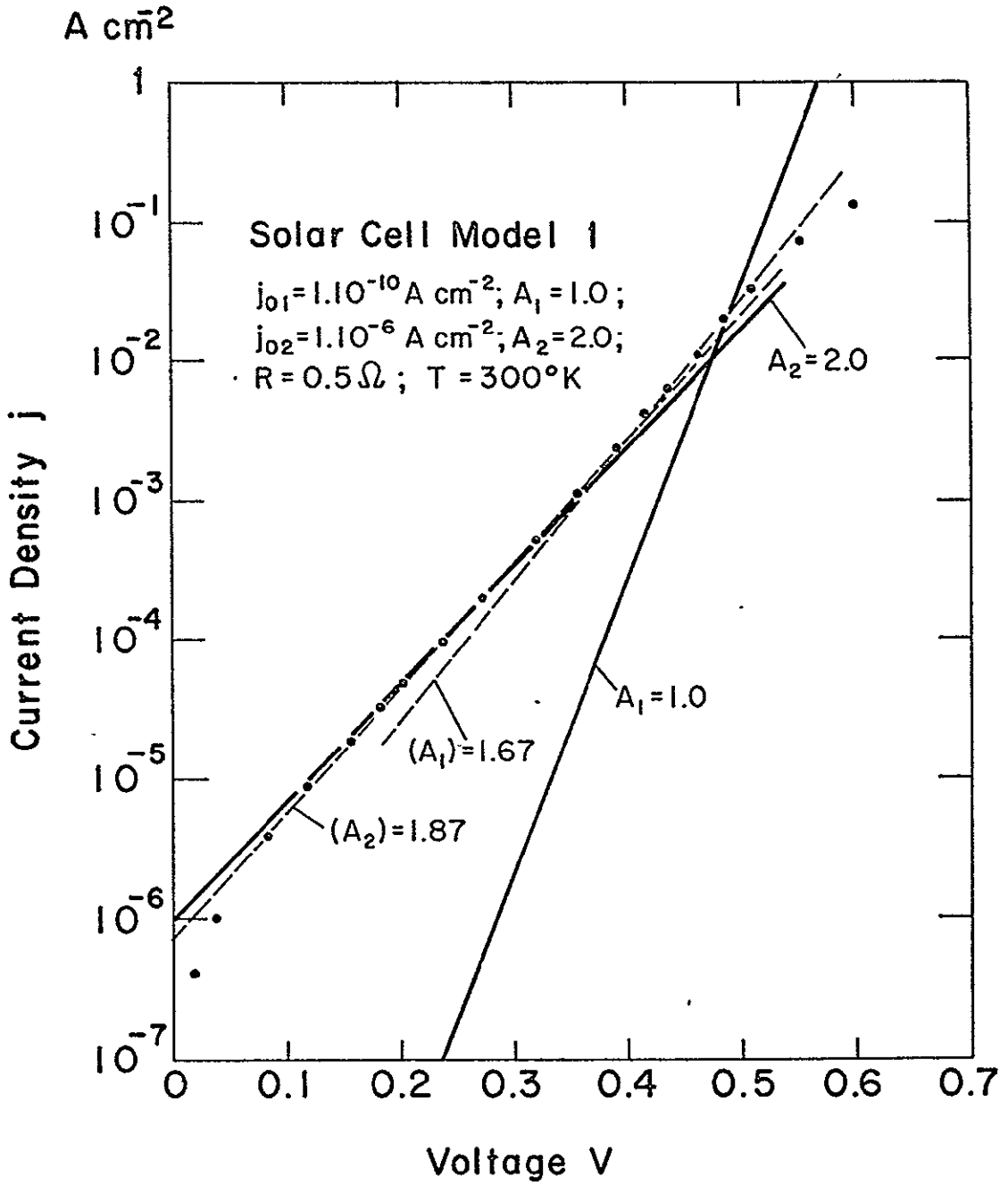

IV-3 The current-voltage characteristic of Model-1, together with the two straight lines representing its generating terms (A_1=1.0 and A_2=2.0), as well as with tangents to the straight line portions of the characteristic.

MODEL 2

Two-Exponential Current-Voltage Characteristic

$I_{01} = 1 \cdot 10^{-10}$ Acm^{-2}; $A_1 = 1.0$; $I_{02} = 1 \cdot 10^{-7}$ Acm^{-2} ; $A_2 = 2.0$; $R = 0.5$

V_D	$I_{01}\left[\exp\left(\frac{qV_D}{A_1 kT}\right) - 1\right]$	$I_{02}\left(\frac{qV_D}{A_2 kT}\right)$	$-I_{02}$	I	V
0.01792	$1.0 \cdot 10^{-10}$	$1.4142 \cdot 10^{-7}$	$-1.0 \cdot 10^{-7}$	$4.152 \cdot 10^{-8}$	
0.03584	3.0	2.0	-1.0	$1.003 \cdot 10^{-7}$	
0.08321	$2.4 \cdot 10^{-9}$	5.0	-1.0	4.024	
0.11904	9.9	$1.0 \cdot 10^{-6}$	-1.0	9.099	
0.15488	$3.99 \cdot 10^{-8}$	2.0	-1.0	$1.940 \cdot 10^{-6}$	
0.2023	$2.499 \cdot 10^{-7}$	5.0	-1.0	5.150	
0.2381	9.999	$1.0 \cdot 10^{-5}$	-1.0	$1.090 \cdot 10^{-5}$	
0.2560	$2.0 \cdot 10^{-6}$	1.414	-1.0	1.604	
0.2797	5.0	2.236	-1.0	2.726	
0.2976	$1.0 \cdot 10^{-5}$	3.162	-1.0	4.152	
0.3155	2.0	4.472	-1.0	6.462	
0.3392	5.0	7.071	-1.0	$1.261 \cdot 10^{-4}$	0.3393
0.3571	$1.0 \cdot 10^{-4}$	$1.0 \cdot 10^{-4}$	-1.0	1.999	0.3572
0.3750	2.0	1.414	-1.0	3.413	0.3752
0.3987	5.0	2.236	-1.0	7.235	0.3991
0.4167	$1.0 \cdot 10^{-3}$	3.162		$1.316 \cdot 10^{-3}$	0.4174
0.4346	2.0	4.472		2.447	0.4358
0.4583	5.0	7.071		5.707	0.4612
0.4762	$1.0 \cdot 10^{-2}$	$1.0 \cdot 10^{-3}$		$1.100 \cdot 10^{-2}$	0.4817
0.4941	2.0	1.41		2.141	0.5048
0.5178	5.0	2.24		5.224	0.5439
0.5357	$1.0 \cdot 10^{-1}$	3.16		$1.032 \cdot 10^{-1}$	0.5873
0.5536	2.0	4.47		2.045	0.6559
0.5773	5.0	7.07		5.071	0.8309

TABLE IV-2

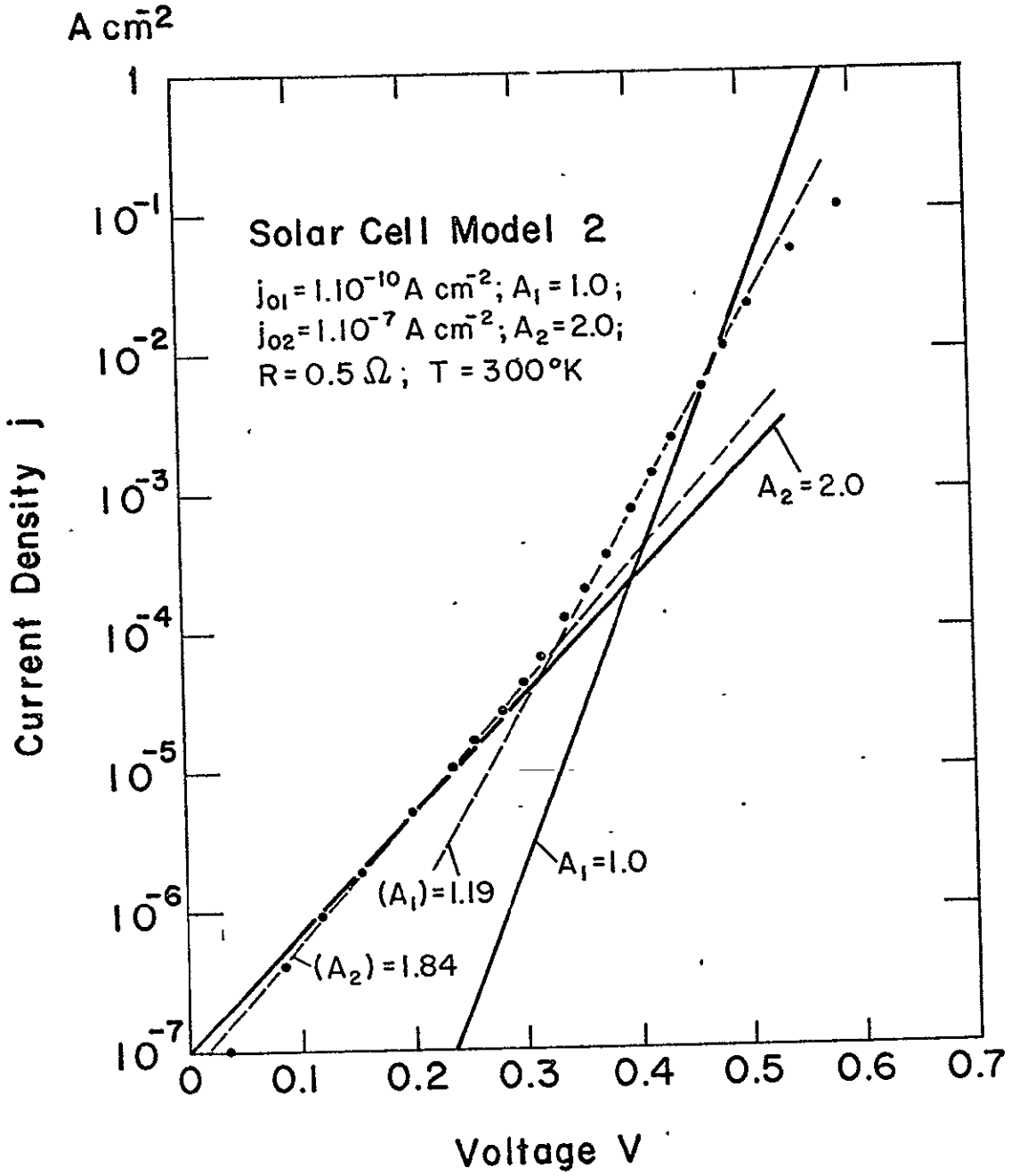

Fig. IV-4 The current-voltage characteristic of Model-2, together with the two straight lines representing its generating terms ($A_1 = 1.0$ and $A_2 = 2.0$), as well as with tangents to the straight line portions of the characteristic.

Subsection 3 then reports further work on a computer program (called VI CHAR for voltage-current characteristic) to ease the interpretation of such experimental data. The mathematical background for this program was provided in section IV of the previous semi-annual report.

It is thus evident that considerable care needs to be taken, both in the acquisition of the experimental data and in their interpretation. Manual interpretation of the two-exponential characteristic leads to a time consuming iteration process. Here, the computer program VI CHAR has proven to be an extremely valuable tool, providing not only considerable time savings, but also an accuracy in data evaluation not matchable in the manual process. More on this subject is contained in the next subsection.

3. The Computer Program VICHAR

In section IV of the first semi-annual report, work-in-progress on a computer program for the evaluation of the five constants, (including series resistance) in the "two-exponential" current voltage characteristics of solar cells has been discussed. Further work on this program (called VICHAR) has been performed in the present reporting period, with the result that considerable confidence in the accuracy and usefulness of this approach have been gained. As a consequence, the work on the generation of this program can be considered completed, with its extensive application as a tool in the future research on current-voltage characteristics indicated.

A program of the mentioned purpose is really useful only, if it will arrive at correct answers for every realistic case of experimental data, without any actions by the computer operator beyond initiating the input. This condition was not fulfilled for a long time due to the fact that the approach is rather sensitive to deviations from their true values of the constants in the exponents. This is particularly the case for R, the value of the series resistance. As long as the estimated (or starting) values for the five constants, or their corrected values in the early iteration steps, are not reasonably close to the ultimate values represented by the experimental data, there is a tendency in the program to over-correct, resulting in possible divergence rather than convergence, to arrive at exponents greater than provided for in the computer, (particularly at low temperatures), or at negative values of R or the j_0's. A substantial number of safeguards have therefore now been built into the program, which has resulted in considerably greater complexity than contained in the original version.

As one of these safeguards, the program hunts for the most rapid convergence by cutting all the correction values resulting from solution of the matrix sequentially in half, down to 2^{-10}. Similarly, it avoids using negative values of resistance or saturation current. Further, the program limits the exponents in magnitude to that permitted in the IBM 360 system (10^{+76}), and if it cannot find convergence with an estimated starting value for series resistance, it will try with up to 5 other values. As a result, the program has lately run to completion on all sets of input data, which reasonably closely represent a two-exponential diode characteristic as expressed by equations 2, 5, and 6 in section IV of the first semi-annual report. The program has proven rather sensitive to this condition, rejecting data containing erroneous points, but has found convergence on input data containing only one exponential or R=0.

Figure IV-5 presents an abridged flow chart of the present program, showing its essential features. VICHAR can be used to determine either all 5 constants, 4 constants, by entering predetermined values for either series resistance R, as may be obtained from separate measurement, or for A_1, (called A1 in program language (WATFIV)), or 3 constants, by entering values for both R and A_1. Accordingly, the program has to solve systems of 5, 4, or 3 simultaneous equations, respectively. For this purpose, either 30 constants (5 by 6 matrix), 20 constants (4 by 5 matrix) or 12 constants will be computed. The 3 to 5 correction values ORANS (Y) are found by solution of the simultaneous equations through diagonalization of the matrix in subroutine SIMUL. The quality of fit between the experimental data and the theoretical two-exponential characteristic at any stage in the iteration process is determined by the second moment of deviation (sum of the squares), evaluated in function ERR. Application of the correction values to either the estimated (or starting) values (ending with - EST) for the 3 to 5 constants to be determined, or to the values of the constants resulting from prior corrections, is made in subroutine USANS.

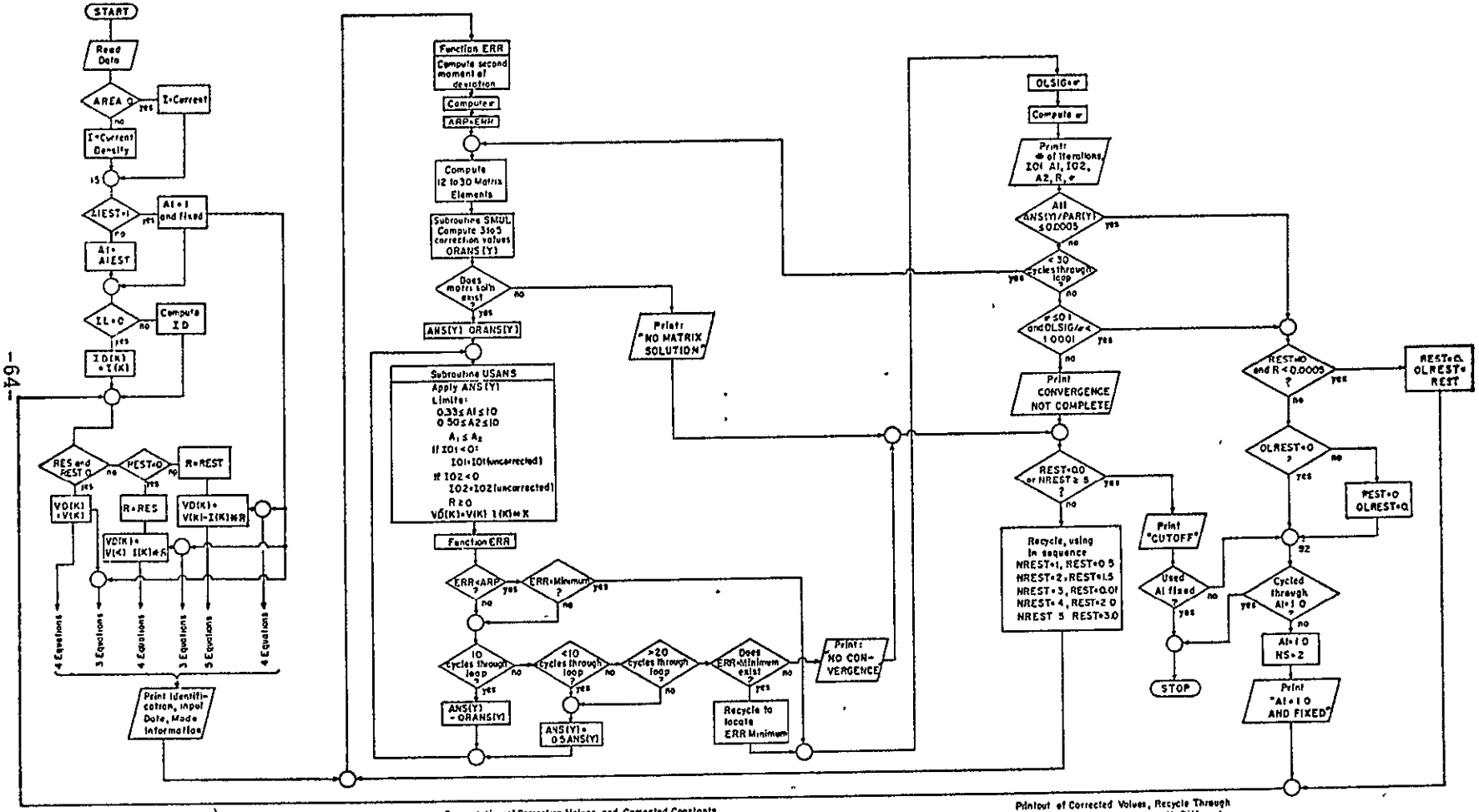

Preparation of Input Data, Determination of Mode of Operation

Computation of Correction Values and Corrected Constants in One Step of Iteration, Determination of Convergence

Printout of Corrected Values, Recycle Through Next Iteration Step or Restart with Different Estimated Value of R; Determination of Completion of Convergence or Cutoff, Recycle with Fixed Value of A1

IV-1 Abridged flow-chart of TSLMAS, showing the key steps in the program

Most of the remainder of the program is devoted to assuring convergence, recycling, etc., as discussed previously. Finally, the program in its present form, after having been run to determine a value for A_1, will recycle with the fixed value $A_1=1.0$.

The convergence criteria for ending the iterations are: no relative change in any of the constants by more than 0.0005 in the last iteration step, or, after 30 iteration steps, the standard deviation between all input data and the two-exponential characteristic with the computed constants is less than 10% and has not changed more than 0.0001 in the last iteration step.

It may be noted that all effort in developing the program has been directed towards its performing the required function, without any attention paid to an elegant approach or lowest cost execution.

As a significant test of the program VI CHAR, the IV data of Model 1 and Model 2, discussed in subsection IV-2 above, have been subjected to its evaluation. On Model 1, the program took 22 iteration steps to arrive at $A_1=0.9993$ and $j_{01}=0.985\cdot10^{-10}$. A_2 was 1.9995, with $j_{02}=0.9989\cdot10^{-6}$, and R=0.5001. The standard deviation between the entered data points and the theoretical curve having the resulting parameters, was $7\cdot10^{-4}$. With the exception of j_{01}, all values are accurate to the fourth significant digit. Similarly, on Model 2, the data were reproduced to the fourth significant digit. Again, j_{01} had a slightly larger error, and the standard deviation was $8\cdot10^{-4}$ in this case.

Two other tests were run on the models, one of them using Model 1 data without series resistance. This is equivalent to using junction data instead of terminal data. The program came to convergence within 10 iteration steps, again finding the original parameters to the fourth significant figure except for j_{01}, which had a 2% error, and with a standard deviation of $5\cdot10^{-4}$. In the other test, only one exponential term, the one

with A_1=1.0, was used, but including series resistance R=0.5 Ohm, (called Model 3). Here, the program surpressed j_{02} to a sufficiently small value, to eliminate the influence of the second exponential term. Again, the values of j_{01}, A_1, and R were reproduced to better than four significant digits, with a standard deviation of $9 \cdot 10^{-4}$.

These tests with the model data have shown clearly that the program VICHAR is capable of reproducing the five constants which were used to generate the input data, with essentially the accuracy of the original data. Thus, the program does not only provide a speedy tool for the evaluation of the five constants, but, moreover, provides an accuracy which cannot be matched by the manual iteration process.

An additional interesting test was accidentally performed, which has shed more light on the question of interpretation of erroneous data. In preparing the card deck for Model 1 without series resistance, one card from the deck with series resistance was left in the new deck. It had a relative error in voltage of approximately 4.10^{-5} compared to the new card, and was left out of sequence in the deck. Both of these facts should not influence the results significantly. Further, a keypunch error had occurred on the 34.14 m A current value, resulting in 31.0 m A. The error was corrected, but the faulty card left in the deck. Since the deck had 2 cards more than expected, the computer did not use the last 2 cards, for current values of 244.7 and 510.7 m A. As a result, A_1 came out 5.7% too high, and j_{01} was high by a factor of 2.53. A_2 and j_{02} differed only in the 4th significant digit, while R was correct. The standard deviation was 4.4%, instead of $4.7 \cdot 10^{-4}$ obtained with the correct deck.

Instructions for use of the program VICHAR are included as Appendix I to this report. Figures IV-6 and IV-7 show two typical pages of computer printout, the first listing the instructions given and the input data, as well as their correction to dark diode junction data, using either an entered value

```
DEVICE NUMBER =  MODEL 1
AREA NOT GIVEN

PRINTOUTS IN A FOR I, OHM FOR R

DARK DIODE, TERMINAL DATA
RESISTANCE UNKNOWN

TEMPERATURE =  300.00
NUMBER OF DATA PAIRS =  20
```

VK	IK	VDK	IDK
0.17920D-01	0.41420D-06	0.17920D-01	0.41420D-06
0.35840D-01	0.10000D-05	0.35839D-01	0.10000D-05
0.83210D-01	0.40000D-05	0.83206D-01	0.40000D-05
0.11904D 00	0.90000D-05	0.11903D 00	0.90000D-05
0.15488D 00	0.19010D-04	0.15486D 00	0.19010D-04
0.20230D 00	0.49250D-04	0.20225D 00	0.49250D-04
0.23810D 00	0.10000D-03	0.23800D 00	0.10000D-03
0.27400D 00	0.20300D-03	0.27380D 00	0.20300D-03
0.32160D 00	0.52400D-03	0.32108D 00	0.52400D-03
0.35760D 00	0.10990D-02	0.35650D 00	0.10990D-02
0.39420D 00	0.23990D-02	0.39180D 00	0.23990D-02
0.41880D 00	0.41610D-02	0.41464D 00	0.41610D-02
0.43780D 00	0.64720D-02	0.43133D 00	0.64720D-02
0.46430D 00	0.12070D-01	0.45223D 00	0.12070D-01
0.48620D 00	0.20000D-01	0.46620D 00	0.20000D-01
0.51120D 00	0.34140D-01	0.47706D 00	0.34140D-01
0.55400D 00	0.72360D-01	0.48164D 00	0.72360D-01
0.60150D 00	0.13160D 00	0.46990D 00	0.13160D 00
0.67600D 00	0.24470D 00	0.43130D 00	0.24470D 00
0.86270D 00	0.57070D 00	0.29200D 00	0.57070D 00

IV-6 Printout page resulting from program VICHAR, showing the input data, in this case for Model-1.

ITER'N	ID1	A1	ID2	A2	R	SIGMA
INIT'L	0.5CC00D-1C	1.CCCCC	C.20000D-05	2.5CCCC	1.C0000	0.60946D 0C
1	0.64595D-1C	1.01722	C.19913D-05	2.49654	0.96415	0.60768D 0C
2	0.82794D-1C	1.03431	C.19828D-05	2.49317	0.92962	0.60573D 0C
3	0.1C522D-C9	1.05115	C.19745D-05	2.48988	0.89655	0.60360D 0C
4	0.13248D-C9	1.06766	C.19662D-05	2.48668	0.86505	0.60130D 0C
5	0.19787D-09	1.10029	C.19500D-05	2.48044	0.80538	0.59859D 0C
6	0.92815D-C9	1.41787	C.18238D-05	2.43355	0.36915	0.59732D 0C
7	0.92815D-C9	1.19540	C.18074D-05	2.42230	0.41979	0.42080D 0C
8	0.12815D-C8	1.15656	C.13169D-05	2.21156	0.47765	0.16710D 0C
9	0.97843D-C9	1.13928	C.12693D-05	2.17999	0.48055	0.15656D 0C
10	0.75491D-C9	1.12302	C.12295D-05	2.15356	0.48314	0.14671D 0C
11	0.59213D-C9	1.10801	C.11962D-05	2.13138	0.48544	0.13702D 0C
12	0.47401D-C9	1.09439	C.11682D-05	2.11268	0.48745	0.12727D 0C
13	0.388CCD-C9	1.08220	C.11445D-05	2.09687	0.48920	0.11742D 0C
14	0.32480D-09	1.07141	C.11244D-05	2.08344	0.49071	0.10760D 0C
15	0.27780D-C9	1.06194	C.11073D-05	2.07201	0.49202	0.97966D-01
16	0.20692D-C9	1.04556	C.10781D-05	2.05255	0.49425	0.86726D-01
17	0.16748D-C9	1.03314	C.10571D-05	2.03856	0.49588	C.72125D-01
18	0.12125D-C9	1.01514	C.10267D-05	2.01833	0.49821	0.52619D-01
19	0.94226D-1C	0.99825	C.99829D-06	1.99924	0.50027	0.98831D-02
20	0.98487D-1C	0.99934	C.99888D-06	1.99946	0.50009	0.76224D-03
21	0.98507D-1C	0.99931	C.99888D-06	1.99946	0.50010	0.70471D-03
22	0.98507D-1C	0.99931	C.99888D-06	1.99946	0.50010	0.70471D-03

IV-7 Printout page resulting from program VICHAR, showing the results, in this case for Model-1.

for series resistance R or the estimated value REST, and an entered value for the light generated current IL, if applicable. Fig. IV-7 contains the results of each iteration step, starting with the estimated values in the first line, and ending with the final values for the 5 constants, after the final convergence criteria have been satisfied. The first column contains the number of the iteration steps before printout of that line, and the last column shows the standard deviation SIGMA achieved with the constants shown on the same line in the remaining columns.

The discussions relative to Fig. IV-2 have shown that 2 data points off the characteristic can cause no-convergence. The accidental test with the faulty deck, discussed above, showed that a 10% error in one data point can cause an increase of about 4% in the standard deviation. These are indications of the great sensitivity of the method to errors in the input. From other tests, the conclusion has been reached that results with standard deviations above 10% should definitely be considered as insufficient convergence, requiring examination of the input data. Also, the input data shall span from at least 50mV to above 100m Acm^{-2}, with at least 2, but preferably 3 data points per decade. Maximum errors in input data of 0.1% for voltage and 1% for current should be strived for. It may be noted that a 0.1% error in voltage at 0.6V corresponds to a 2.4% current error. Combined with a 1% current error (independent measurement), this means a maximum deviation from the true value of 3.4%, or a probable deviation of 1.7%. Thus, a standard deviation for the entire data group around 1.5% might be expected.

4. Conclusion:

The program VICHAR has proven to be an excellent tool for the evaluation of experimental data of the current-voltage characteristic of silicon solar cells, and possibly other pn-junction devices. It does not only provide a tremendous labor saving compared to the earlier manual method, but, also yields much greater accuracy, provided the input data are of sufficient quality. As the result of the availability of this new tool for the evaluation of the IV characteristics, it has become clear that further studies will require more accurate experimental data, than have generally been used up to now. However, one conclusion can already be drawn from the limited amount of experimental data evaluated with the computer program: the small standard deviations (2 to 4 %), with which the two-exponential current-voltage relationship has been fitted to the experimental curves, strongly suggests that the two-exponential characteristic actually is the analytical relationship which describes the experimental data. Up to this point, the doubt existed that the two-exponential characteristic might be nothing but a reasonably good approximation to the experimental data, which might otherwise be better described by a different mathematical relationship. However, with this close reproduction of the experimental data, and in view of the great sensitivity to data deviations discussed earlier, considerable confidence exists now that the two-exponential relationship is actually the proper analytical expression for the IV characteristic of silicon solar cells and perhaps for many other pn-junction devices.

In consequence, the next step will be to re-examine the existing theories on pn-junction current flow for their capability to provide the required two-exponential IV characteristic. If they should not be capable of describing this characteristic, the search would have to go much deeper, into basic phenomena and their relationship to the IV-characteristic.

V IMPROVEMENT OF THE DIFFUSED REGION COLLECTION EFFICIENCY

It had been predicted (ref.1), that a 17% improvement in collection efficiency should be obtainable by reduction of the surface recombination velocity of the diffused region and by reduction of the diffused region thickness. Later design calculations, included in the first semi-annual report, indicated that the diffused region thickness reduction might not be necessary, if the quality of the material parameters in the diffused region should be better than originally thought, or if it could be improved by a relatively small margin. It was expected, that some preliminary experimental work towards the verification of this prediction would be carried out.

As the planning for this experimental program got under way at the beginning of this year, it was learned accidentally, that a program with the same objective, spawned by this author's prediction, was well under way at Comsat Laboratories uner the direction of Dr. J. Lindmayer. It was also learned that preliminary results appeared hopeful. Since more extensive and conclusive results were expected within a few months, the preparations for our own experimentation were slowed down, in order to avoid unnecessary duplication.

It has now been learned from Dr. Lindmayer, that the experiments have been very successful. The collection efficiency of the silicon cells has been improved by about 20%, based, however, on a cell of thinner base region thickness than used in the calculations. The lower base region thickness implies a lower long wavelength collection efficiency and thus, a lower total collection efficiency base for the improvement. Further, the anti-reflection coating was heavily blue shifted, with a resulting higher reflection in the long wavelength region, resulting in an additional effect of the same consequences as the reduced base region thickness. Thus, the achieved improvement is just of the right magnitude.

Details of the method by which the improvement was achieved are still proprietory information of Comsat Laboratories, but are in preparation for publication. It has also been found there, that the conventional process providing the anti-reflection coating does not permit full realization of the improved short wavelength response achieved by the diffused region parameter improvement. Further development of suitable anti-reflection coatings is still under way at Comsat Laboratories, which has a publication in preparation on the subject of the short wavelength response improvement.

It may also be noted with interest, that the collection efficiency improvement in the short wavelength region has been found to be extremely radiation resistant in preliminary tests at Comsat Laboratories. Thus, the improvement in overall collection efficiency of the silicon solar cell has been accompanied by a new level of radiation hardness. This also is in line with the expectations.

In view of this work performed at Comsat Laboratories, it would not appear sensible to proceed with the program as originally planned. Rather, further disclosure of data from Comsat Laboratories should be awaited. Following evaluation of these data, a modified program of experimental investigation may then be undertaken.

APPENDIX 1

Instructions for Use of Program VICHAR

1. Cards of Data Package:

Start card: /GO in columns 1 to 3

Card 1: Estimated or starting values for

I_{01} (I$\emptyset$IEST), A_1 (A1EST), I_{02} (1$\emptyset$EST), A_2 (A2 EST),

and R (REST), in this sequence. I_0 in Acm^{-2} or A, R in Ohm.

FORMAT:

I_{01} = double precision floating decimal (D20.14), start column 1;

A_1 = fixed decimal (F10.6), start column 21;

I_{02} = double precision floating decimal (D20.14), start column 31;

A_2 = fixed decimal (F10.6), start column 51;

R = fixed decimal, (F10.6), start column 61.

Card 2: Number (NSYS) of VI - characteristics to be processed.

FORMAT: Integer, columns 1-5 (units in column 5, tens in column 4, etc.)

The following cards have to be provided for for each VI - characteristic to be processed.

Card 3: Device temperature T, in degrees K;

FORMAT: fixed decimal, columns 1-20

Card 4: Number of fixed resistance values to be used (NRES), fixed resistance values (RES) in Ohm; (up to 15 values).

FORMAT: NRES: integer columns 4-5 (units in column 5, tens in 4, etc.)

RES: fixed decimal (F10.6), 7 times, starting column 11, additional 8 times on continuation card, starting

Card 5: Light generated current I_L (IL), in Acm^{-2} or A, when illuminated VI-characteristic is to be evaluated. Otherwise no entry on card.

FORMAT: fixed decimal, columns 1-20.

Card 6: Device label (identification) (DEV), number of data pairs in VI-characteristic (ND), junction area in cm^2 (AREA), in this sequence.

FORMAT: alphameric columns 1 to 16 for DEV; integer columns 21 and 22 for ND (units in column 22); double precision floating decimal for AREA, columns 31 to 50.

ND cards: voltage (V) in Volt and current (I) in Acm^{-2} or A, in this sequence.

FORMAT: V: fixed decimal columns 1 to 20,
I: fixed decimal columns 21-40.
Each data pair one card.

End Card: / END columns 1 to 4.

2. All current values to be entered either in Acm^{-2} or in A.
3. A value for AREA should be entered, when current data (in A) are entered and evaluation in current density (in Acm^{-2}) is desired (normalization to unit area).
4. If terminal voltage data are entered, at least one value for either REST or RES has to be entered. Otherwise, the input data will be treated as junction voltage data.
5. If evaluation with a fixed resistance value is to be carried out, no value (or $\emptyset.\emptyset$) is to be entered for REST.
6. If evaluation with a fixed value of $1.\emptyset$ for A_1 is to executed, no value (or $\emptyset.\emptyset$) for AIEST is to be entered.
7. Any combination of the above is permitted.

VI PROJECT STATUS

1. Point 1 of the program is completed.
2. Point 2 has been delayed as explained in section V of this report.
3. Point 3 is in progress. Contacts to material suppliers have been made and answers are starting to be received.
4. As additional work, the computer program VICHAR for evaluation of the 5 constants is the 2-exponential current-voltage characteristic is completed.
5. As additional work, a study of the saturation current contribution from the base region, using a 2-layer model with drift fields, similar to the one evaluated for collection efficiency, is well under way.
6. As additional work, the data resulting from point 1 of the milestone chart have been re-cast to form the beginning of a "Silicon Solar Cell Design Handbook".

VII PLANS FOR NEXT REPORTING PERIOD

1. Whenever appropriate, redesign experimentation according to section point 2 of the milestone chart.

2. Proceed with point 3a, of the milestone chart and start point 3b.

3. Complete the study of saturation current contribution from the base region.

VIII SUMMARY, CONCLUSIONS, RECOMMENDATIONS

1. The collection efficiency part of a "Silicon Solar Cell Design Handbook" has been completed. For this purpose, the total solar flux is divided into the parts absorbed in the various region of the solar cell (diffused region, base region, etc.),(function of region thickness), and the collection efficiency from these regions determined as function of the relevant physical and material parameters.

2. Additional data sets for base region collection efficiency were obtained for various values of distance from the light exposed surface to the interface plane between depletion region and base region.

3. A relationship was derived to evaluate the saturation current contribution from the diffused region for arbitrary surface recombination velocity and arbitrary thickness of the diffused region. It was found that a "form-factor" applied to the standard saturation current formula best describes the influence of these parameters.

4. Using the relationship mentioned under 3 , it was determined that:
   a. The proximity of the ohmic contact as such (excluding process caused effects, such as diffusion of metals) to the depletion region (pn junction) has no significant effect in present silicon solar cells due to the high surface recombination velocity at the exposed surface.
   b. In future cells of low surface recombination velocity, saturation current below the values predicted from the diffusion theory for thick layers (the commonly used relationship) can be obtained. This can result, e.g., in an easing of the requirement for good minority carrier lifetime in the diffused region.

c. If case 4b., is fulfilled, it may be necessary to provide a deeper diffused guard layer under the ohmic contacts.

5. To investigate the influence on saturation current (and thus on the IV-characteristic) of measures found to improve collection efficiency in thin cells (such as a drift field in front of the back contact), a base layer model for saturation current computation was derived in analogy to the 2 - layer model including field terms for the collection efficiency.

6. Using the model of 5., above, a multivariable "experiment" was completed, but not yet fully evaluated. Preliminary inspection seems to indicate however, that whatever improves collection efficiency, also lowers the saturation current.

7. The computer program VICHAR for the evaluation of the 5 constants in the two-exponential current-voltage characteristic from experimental data has been completed. It not only provides labor saving, but also an accuracy not obtainable by other methods.

8. Experimentation carried out at Comsat Laboratories has achieved the improvement of short wavelength collection efficiency predicted from this analytical work. It has also been found there that the present anti-reflection coatings do not permit full utilization of this improvement, resulting in efforts there towards development of a better AR coating.